ACCELERATED IMPLEMENTATION OF INTELLIGENT COMPACTION TECHNOLOGY FOR EMBANKMENT SUBGRADE SOILS, AGGREGATE BASE, AND ASPHALT PAVEMENT MATERIALS: SR-25 WEST LAFAYETTE, INDIANA

Prepared By

David J. White, Ph.D.
Pavana KR. Vennapusa, Ph.D.
Heath Gieselman, M.S.

Earthworks Engineering Research Center (EERC)
Department of Civil Construction and Environmental Engineering
Iowa State University
2711 South Loop Drive, Suite 4600
Ames, IA 50010-8664
Phone: 515-294-7910
www.eerc.iastate.edu

April 2011

TABLE OF CONTENTS

LIST OF FIGURES

LIST OF TABLES

Acknowledgments

LIST OF symbols

a	Theoretical vibration amplitude (eccentric moment divided by the drum mass)
A'	Machine acceleration
AFC	Automatic feedback control
b	Machine internal loss coefficient used in MDP calculation
b_0	Intercept in a linear regression equation
b_1, b_2, b_3	Regression coefficients
C	Semivariogram scale
C_0	Semivariogram nugget
$C+C_0$	Semivariogram sill
CBR	California bearing ratio (weighted average to compaction layer depth)
COV	Coefficient of variation (calculated as the ratio of mean and standard deviation)
DPI	Dynamic cone penetration index
d_0	Measured settlement under plate
D_{10}	Particle size corresponding to 10% passing
D_{30}	Particle size corresponding to 30% passing
D_{60}	Particle size corresponding to 60% passing
E	Elastic modulus
E_{LWD-Z3}	Elastic modulus determined from 300-mm plate Zorn light weight deflectometer
f	Vibration frequency
F	Shape factor
g	Acceleration due to gravity
G_s	Specific gravity
GPS	Global positioning system
h	Separation distance
IC-MV	Intelligent compaction measurement value
LL	Liquid limit
m	Machine internal loss coefficient used in MDP calculation
MDP	Caterpillar Machine drive power
MDP*	See description in text

MV	Measurement value
n	Number of test measurements
P_g	Gross power needed to move the machine
PI	Plasticity index
PL	Plastic limit
Point-MV	In-situ point measurement value
r	Radius of the plate
R	Semivariogram range
R^2	Coefficient of determination
v	Roller velocity
w	Moisture content determined from Humboldt nuclear gauge
w_{opt}	Optimum moisture content
W	Roller weight
μ	Statistical mean
σ	Statistical standard deviation
σ_0	Applied stress
η	Poisson's ratio
γ_d	Dry unit weight determined from Humboldt nuclear gauge (NG)
γ_{dmax}	Maximum dry unit weight
$\gamma(h)$	Semivariogram

Introduction

This report presents results from a field investigation conducted on the State Route 25 (SR-25), which is a new highway alignment extending from I-65 to CR750E north of Buck Creek, West Lafayette, Indiana. The machine configurations and roller-integrated measurement systems used on this project included: a Caterpillar CS56 smooth drum with a padfoot shell kit and a Caterpillar CS563E smooth drum vibratory roller, both equipped with machine drive power (MDP) intelligent compaction (IC) measurement technology. The two machines were equipped with real time kinematic (RTK) global positioning system (GPS) and on-board display and documentation systems. The project involved constructing and testing six test beds consisting of cohesive and granular embankment fill materials. The intelligent compaction (IC) measurement values (MVs) were evaluated by conducting field testing in conjunction with a variety of in-situ testing devices measuring density, moisture content, California bearing ratio (CBR), and elastic modulus. An open house was conducted near the end of the field investigation to disseminate results from current and previous IC projects. The Indiana department of transportation (INDOT), contractor's personnel, and representatives from the IC roller manufacturers participated in the field testing phase of the project and the open house.

The goals of this field investigation were similar to previous demonstration projects and included the following:

- document machine vibration amplitude influence on compaction efficiency,
- develop correlations between IC measurement values (IC-MVs) to traditional in-situ point measurements (point-MVs),
- compare IC results to traditional compaction operations,
- study IC measurement values in production compaction operations, and
- evaluate IC measurement values in terms of alternative specification options.

This report presents brief background information of the MDP IC measurement technology evaluated in this study, documents the results and analysis from field testing, and documents the field demonstration activities. Regression analysis was performed to evaluate correlations between IC-MVs and in-situ compaction measurements determined using point-MVs. Dry density and moisture content measurements were obtained using INDOT's Humboldt nuclear gauge, modulus measurements were obtained using Zorn light weight deflectometers (LWDs) setup with 300 mm diameter plate, and California bearing ratio measurements obtained from dynamic cone penetrometer (DCP). Geostatistical methods were used to quantify and characterize spatial non-uniformity of the compacted fill materials in the production area using spatially referenced IC-MV data. Position information of IC-MV and point-MV data were recorded with real time kinematic (RTK) global positioning system (GPS) measurements.

The results and correlations provided in this report should be of significant interest to the pavement, geotechnical, and construction engineering community and are anticipated to serve as a good knowledge base for implementation of IC compaction monitoring technologies and various new in-situ testing methods into earthwork construction practice.

Background

Machine Drive Power

Caterpillar CS56 smooth drum with a padfoot shell kit and Caterpillar CS563E vibratory smooth drum IC rollers were used on the project (Figure 1). A digital display unit (Figure 2) employing proprietary software is mounted in the roller cabin for on-board visualization of roller position, IC-MVs, coverage information, amplitude/frequency settings, speed, etc. The rollers were outfitted with a real-time kinematic (RTK) global positioning system (GPS) to continuously record the roller position information. Some key features of the rollers are summarized in Table 1. The padfoot roller (CS56) and the smooth drum roller (CS563E) recorded machine drive power (MDP). Brief descriptions of the MDP IC-MVs is provided in the following discussion.

Table 1. Key features of the IC rollers used on the project

Feature	Caterpillar CS56 and CS563
Drum Type	CS56 – Padfoot shell kit over smooth drum CS563E – Smooth drum
Frequency (f)	30 Hz
Amplitude (a) Settings	Static, 0.90 mm (low amplitude), and 1.80 mm (high amplitude)
IC-MV	MDP_{40} (shown as CCV in the output)
Display Software	AccuGrade^{TM} office
GPS coordinates	Based on local arbitrary coordinates at the base station
Output Documentation	Date/Time, Location (Northing/Easting/Elevation of left and right ends of the roller drum), Speed, CCV, Frequency, Amplitude (theoretical), Direction (forward/ backward), Vibration (On/Off)
Data frequency	About every 0.2 m at the center of the drum (for a nominal $v = 4$ km/h)
Output Export File	*.csv
Automatic Feedback Control (AFC)[a]	No

[a]AFC mode involves automatic adjustment of vibration amplitude and/or frequency during compaction.

MDP technology relates mechanical performance of the roller during compaction to the properties of the compacted soil. Detailed background information on the MDP system is provided by White et al. (2005). Controlled field studies documented by White and Thompson (2008), Thompson and White (2008), and Vennapusa et al. (2009) verified that MDP values are empirically related to soil compaction characteristics (e.g., density, stiffness, and strength). MDP is calculated using Eq. 1.

$$MDP = P_g - Wv\left(Sin\alpha + \frac{A'}{g}\right) - \left(mv + b\right) \tag{1}$$

Where MDP = machine drive power (kJ/s), P_g = gross power needed to move the machine (kJ/s),

W = roller weight (kN), A' = machine acceleration (m/s^2), g = acceleration of gravity (m/s^2), α = slope angle (roller pitch from a sensor), v = roller velocity (m/s), and m (kJ/m) and b (kJ/s) = machine internal loss coefficients specific to a particular machine (White et al. 2005). MDP is a relative value referencing the material properties of the calibration surface, which is generally a hard compacted surface (MDP = 0 kJ/s). Positive MDP values therefore indicate material that is less compact than the calibration surface, while negative MDP values indicate material that is more compacted than the calibration surface (i.e. less roller drum sinkage). The MDP values obtained from the machine were recalculated to range between 1 and 150 and these re-scaled values are referred to as MDP* in this report. While the original MDP values decrease in increasing compaction, the MDP* values increase with increasing compaction.
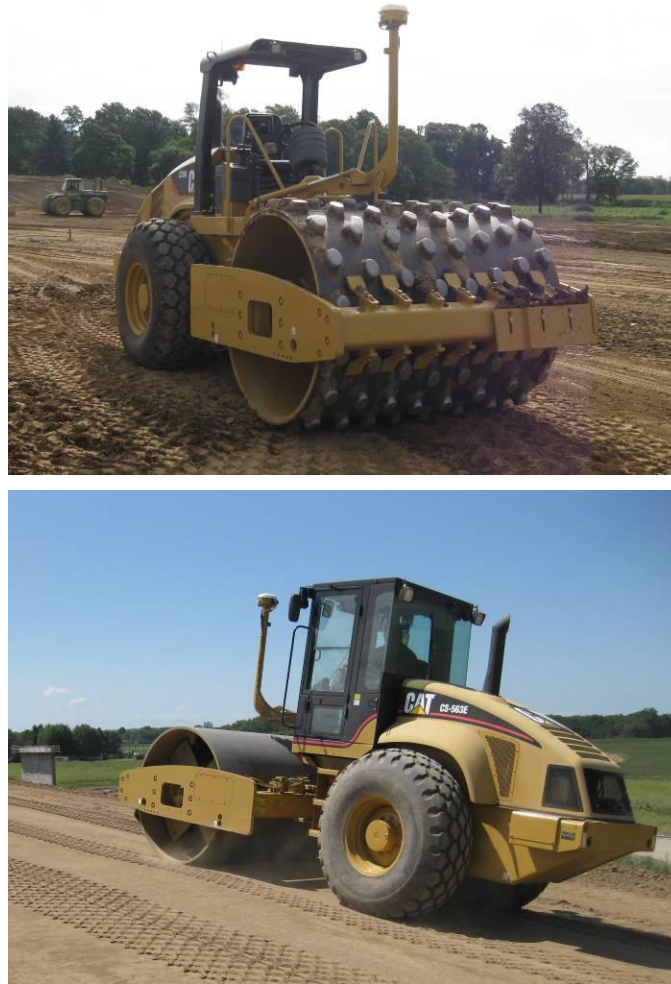
Figure 1. Caterpillar CS56 smooth drum with padfoot shell kit (top) and Caterpillar CS563E smooth drum (bottom) IC rollers used on the project

Figure 2. On board Accugrade display unit showing compaction data in real-time

In-situ Testing Methods

Three different in-situ testing methods were used in this study to evaluate the in-situ soil engineering properties (Figure 3): (a) calibrated Humboldt nuclear gauge (NG) to measure moisture content (w) and dry unit weight (γ_d), (b) dynamic cone penetrometer (DCP) to determine California bearing Ratio (CBR), and (c) Zorn light weight deflectometer setup with 300 mm plate diameter to determine elastic modulus. Assistance with field testing was provided by several INDOT personnel.

DCP tests were performed in accordance with ASTM D695-03 to determine dynamic cone penetration index (DPI) and calculate CBR using Eq. 4. The DCP test results are presented in this report as CBR point values or CBR with depth profiles. When the data is presented as point values, the data represents a weighted average CBR of the top 300 mm depth (i.e., compaction layer thickness).

$$\text{CBR} = \frac{292}{\text{DPI}^{1.12}} \tag{4}$$

LWD tests were performed following manufacturer recommendations (Zorn 2003) and the modulus values were determined using Eq. 5, where E = elastic modulus (MPa), d_0 = measured settlement (mm), η = Poisson's ratio (0.4), σ_0 = applied stress (MPa), r = radius of the plate (mm), F = shape factor depending on stress distribution (assumed as 8/3) (see Vennapusa and White 2009). The LWD modulus results are reported as $E_{\text{LWD-Z3}}$ (Z represents Zorn LWD and 3 represents 300 mm diameter plate).

$$E = \frac{(1-\eta^2)\sigma_0 r}{d_0} \times F \tag{5}$$

4

The Iowa State University Geotechnical mobile laboratory Figure 3 is equipped with Davis Vantage Pro weather station with a Weatherlink datalogger system. Weather data was monitored and recorded every 30 minutes by the datalogger. Air temperature and wind speed recorded during the course of the project are presented in Figure 4. Approximate time of construction and testing of different test beds is shown in Figure 4.

Figure 3. In-situ testing methods: Humboldt nuclear gauge (top left), dynamic cone penetrometer (top middle), and Zorn light weight deflectometer (top right), and Iowa State University geotechnical mobile laboratory (bottom)
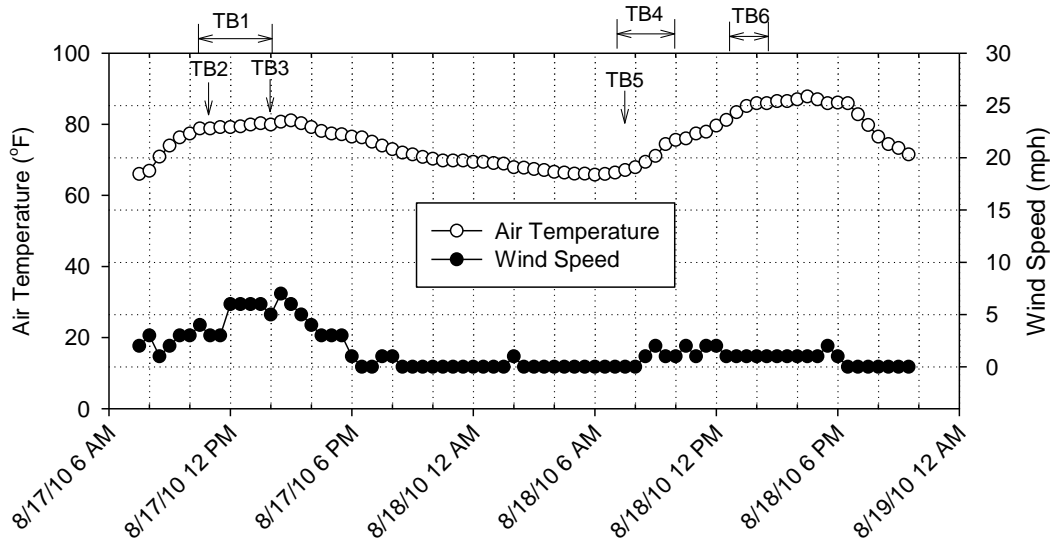
Figure 4. Air temperature and wind speed data

Analysis Methods

Regression Analysis

Simple linear and non-linear regression relationships between IC-MVs and in-situ point measurement values (Point MVs) were developed by spatially pairing the data obtained from the test beds. The analysis was performed by considering point-MVs as "true" independent variables and IC-MVs as dependent variables using the models shown in Eqs. 2 to 3, where b_0 = intercept and b_1, b_2 = regression parameters.

$$\text{Linear model: } IC\text{–}MV = b_0 + b_1 \cdot \text{Point MV} \tag{2}$$

$$\text{Non-linear power model: } IC\text{–}MV = b_1(\text{Point MV})^{b_2} \tag{3}$$

Statistical significance of the independent variable was assessed based on *p*- and *t*-values. The selected criteria for identifying the significance of a parameter included: *p*-value < 0.05 = significant, < 0.10 = possibly significant, > 0.10 = not significant, and *t*-value < -2 or > +2 = significant. The best fit model is determined based on the strength of the regression relationships assessed by the coefficient of determination (i.e., R^2) values. For the analysis and discussion in this report, an R^2 value ≥ 0.5 is considered acceptable following the guidelines from European specifications. A statistical prediction interval approach for determining "target" values from the regression relationships would account for R^2 values in the relationships (see Mooney et al. 2010). A regression relationship with lower R^2 values would result in higher target value and a regression relationship with higher R^2 value will result in lower target values.

Geostatistical Analysis

Spatially referenced IC-MVs provide an opportunity to quantify "non-uniformity" of compacted fill materials. Vennapusa et al. (2010) demonstrated the use of semivariogram analysis in

6

combination with conventional statistical analysis to evaluate non-uniformity in QC/QA during earthwork construction. A semivariogram is a plot of the average squared differences between data values as a function of separation distance, and is a common tool used in geostatistical studies to describe spatial variation. A typical semivariogram plot is presented in Figure 5. The semivariogram $\gamma(h)$ is defined as one-half of the average squared differences between data values that are separated at a distance h (Isaaks and Srivastava 1989). If this calculation is repeated for many different values of h (as the sample data will support) the result can be graphically presented as experimental semivariogram shown as circles in Figure 5. More details on experimental semivariogram calculation procedure are available elsewhere in the literature (e.g., Clark and Harper 2002, Isaaks and Srivastava 1989).

Spherical Semivariogram

$$\gamma(0) = 0$$

$$\gamma(h) = C_0 + C\left[\frac{3h}{2R} - \frac{h^3}{2R^3}\right] ----> 0 < h < R$$

$$\gamma(h) = C_0 + C ----> h > R$$

Range (R)

Semivariogram, γ (h)

Experimental Semivariogram (circles)

Scale, C

Sill C + C_0

Nugget, C_0

Separation Distance, h

Range, R: As the separation distance between pairs increase, the corresponding semivariogram value will also generally increase. Eventually, however, an increase in the distance no longer causes a corresponding increase in the semivariogram, i.e., where the semivariogram reaches a plateau. The distance at which the semivariogram reaches this plateau is called as range. Longer range values suggest greater spatial continuity or relatively larger (more spatially coherent) "hot spots".

Sill, C+C_0: The plateau that the semivariogram reaches at the range is called the sill. A semivariogram generally has a sill that is approximately equal to the variance of the data.

Nugget, C_0: Though the value of the semivariogram at h = 0 is strictly zero, several factors, such as sampling error and very short scale variability, may cause sample values separated by extremely short distances to be quite dissimilar. This causes a discontinuity at the origin of the semivariogram and is described as nugget effect. (Isaaks and Srivastava, 1989)

Figure 5. Description of a typical experimental and spherical semivariogram and its parameters

To obtain an algebraic expression for the relationship between separation distance and experimental semivariogram, a theoretical model is fit to the data. Some commonly used models include linear, spherical, exponential, and Gaussian models. A spherical model was used for data analysis in this report. Arithmetic expression of the spherical model and the spherical variogram are shown in Figure 5. Three parameters are used to construct a theoretical semivariogram: sill ($C+C_0$), range (R), and nugget (C_0). These parameters are briefly described in Figure 5. More discussion on the theoretical models can be found elsewhere in the literature (e.g., Clark and Harper 2002). For the results presented in this section, the sill, range, and nugget values during theoretical model fitting were determined by checking the models for "goodness" using the modified Cressie goodness fit method (Clark and Harper 2002) and cross-validation process (Isaaks and Srivastava 1989). From a theoretical semivariogram model, a low "sill" and longer "range of influence" represent best conditions for uniformity, while the opposite represents an increasingly non-uniform condition. Some of the results presented in this report revealed nested structures with short-range and long-range components in the experimental semivariograms. Nested structures have been observed in geological applications where different physical processes are responsible for spatial variations at different scale (see Chiles and Delfiner 1999). For the cases with nested structures, nested spherical variograms combining two spherical models (with two sill values and two range values) are fit to the experimental semivariogram data.

Experimental Testing

Description of Test Beds

A total of six test beds (TBs) with one cohesive and one granular embankment fill material were constructed and tested as part of this study. A summary of test beds with material conditions and tests performed is provided in Table 2. A summary of material index properties is provided in Table 3. Details regarding construction and testing of each test bed are provided in the following sections. A plan view map showing locations of in-situ testing and roller data from the whole project site is shown in Figure 6.

Table 2. Summary of test beds and in-situ testing

TB	Description	Material	Date	Machine	Total Passes	Amplitude setting, Speed (km/h)*	Notes/In-situ Point Measurements
1	Calibration Test Strip (lane 1)	Granular Embankment Fill	08/17	CAT CS-563E Smooth Drum	4	Low amplitude, 2.5	E_{LWD-Z3}, γ_d, w, and DCP after 0, 1, 2, 4 passes at 5 test locations
	Calibration Test Strip (lane 2)					High amplitude, 2.5	
2	Test Strip	Granular Embankment Fill	08/17		16	Low amplitude, 2.8	E_{LWD-Z3} @ multiple depths below grade
3	Production Area Compaction (66 minutes, 49,586 ft^2)	Granular Embankment Fill (Lift #1)	08/17	CAT CS-563E Smooth Drum	2	Low amplitude, 3.2	E_{LWD-Z3} and DCP after 2 passes in three test areas (20 points (hard area), 16 points(average area), 28 points (soft area)
4	Calibration Test Strip (lane 1)	Cohesive Embankment Fill	08/18	CAT CS-56 Smooth Drum w/ Padfoot Shell Kit	8	Low amplitude, 3.8	E_{LWD-Z2}, γ_d and w, and DCP at seven locations after passes 0 and 8.
	Calibration Test Strip (lane 2)	Cohesive Embankment Fill	08/18		8	Static, 3.8	
5	Test Strip	Cohesive Embankment Fill	08/18	CAT CS-56 Smooth Drum w/ Padfoot Shell Kit	8	Low amplitude for pass 1 and static thereafter, 3.8	E_{LWD-Z2} at 72 test locations
6	Production Area Compaction (104 minutes, 53,189 ft^2)	Sandy Embankment Fill (Lift #2 – contractor operator)	08/18	CAT CS-563E Smooth Drum	4	Low amplitude, 3.8	E_{LWD-Z3}, γ_d, w, and DCP after 4 passes in six test areas:42 LWD, and 7 each γ_d, w, and DCP
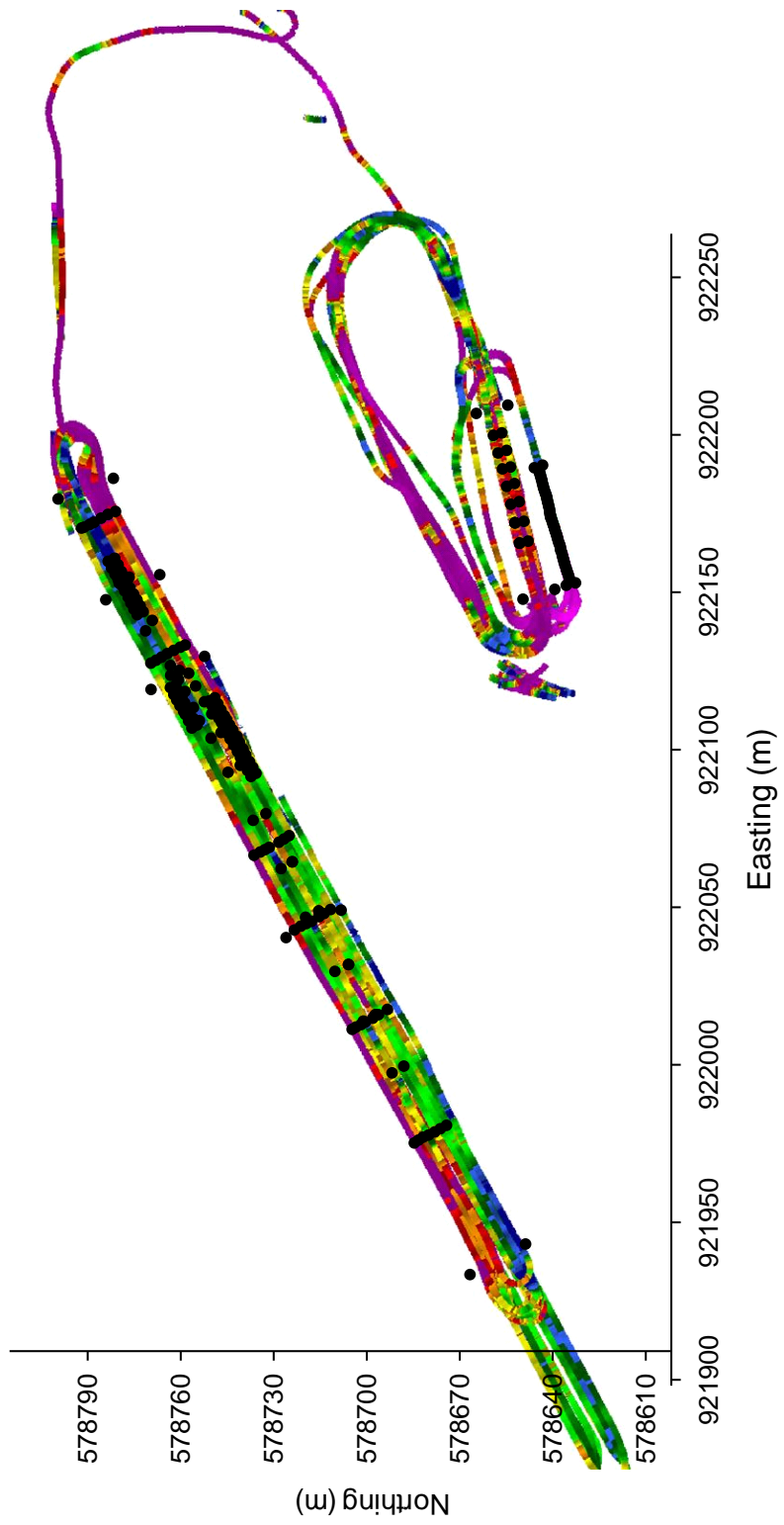
Figure 6. Roller map with in-situ point-MV locations (shown as black circles)

Laboratory Test Results

Grain-size analysis, Atterberg limits, specific gravity, and standard Proctor test results were provided by INDOT and are summarized in Table 3. Grain-size distribution curves are presented in Figure 7. Based on the grain-size analysis and Atterberg test results, the two soils are classified in accordance with the unified soil classification system (USCS) and the American association of state highway and transportation officials (AASHTO) system as shown in Table 3. Standard Proctor test results for the two soils are presented in Figure 8 and Figure 9. The maximum dry unit weight (γ_{dmax}) and optimum moisture content (w_{opt}) results from Proctor tests for the two soils are summarized in 3.

Table 3. Summary of material index properties

Parameter	Cohesive Embankment Fill	Granular Embankment Fill
Grain-Size Analysis Results		
Gravel Content (%) (> 4.75mm)	2.9	4.1
Sand Content (%) (4.75mm – 75μm)	31.2	86.8
Silt + Clay Content (%) (<75μm)	65.9	9.1
D_{10} (mm)		0.08
D_{30} (mm)		0.18
D_{60} (mm)	Not applicable	0.57
Coefficient of Uniformity, c_u		7.13
Coefficient of Curvature, c_c		0.71
Atterberg Limits Test Results		
Liquid Limit, LL (%)	42	Non-Plastic
Plasticity Index, PI (%)	23	
AASHTO Classification	A-7-6(13)	A-3
USCS Classification	CL	SP-SM
USCS Soil Description	Sandy Lean Clay	Poorly graded sand with silt
Specific Gravity, G_s	2.657	2.686
Standard Proctor Test Results (AASHTO T-99)		
γ_{dmax} (kN/m^3)	17.19	18.98
γ_{dmax} (pcf)	109.4	120.8
w_{opt} (%)	17.2	14.2
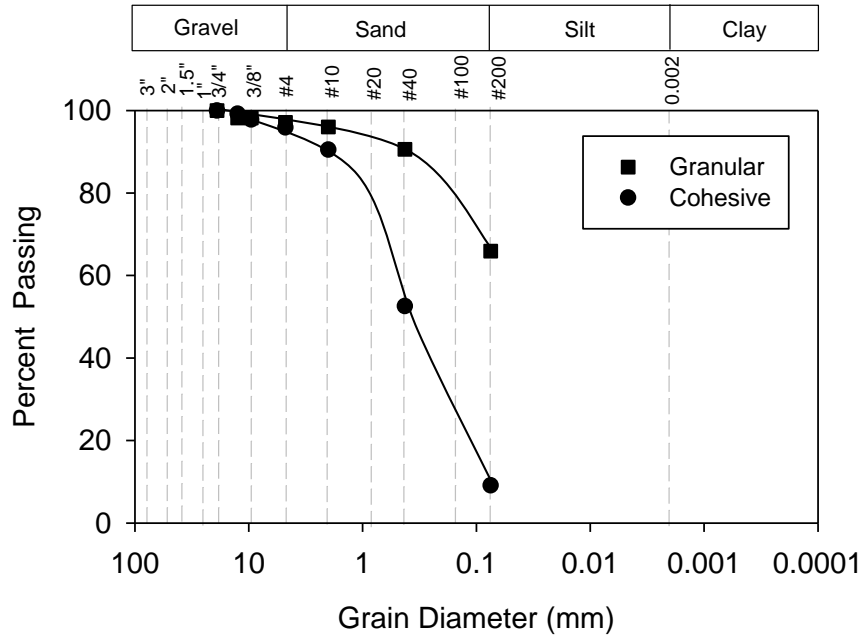
Figure 7. Grain size distribution curves of the two soils tested in this study
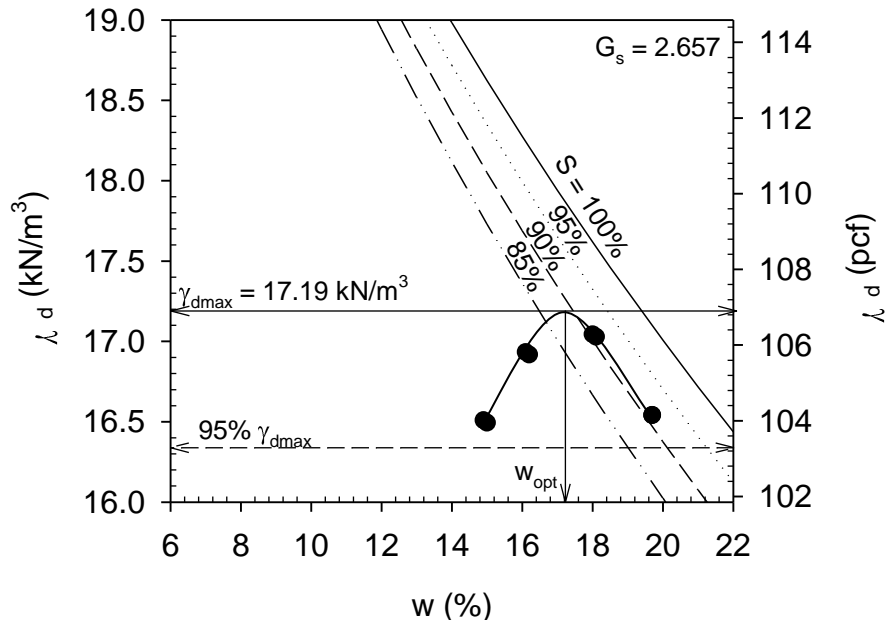
Figure 8. Results of laboratory standard Proctor test on cohesive embankment fill material
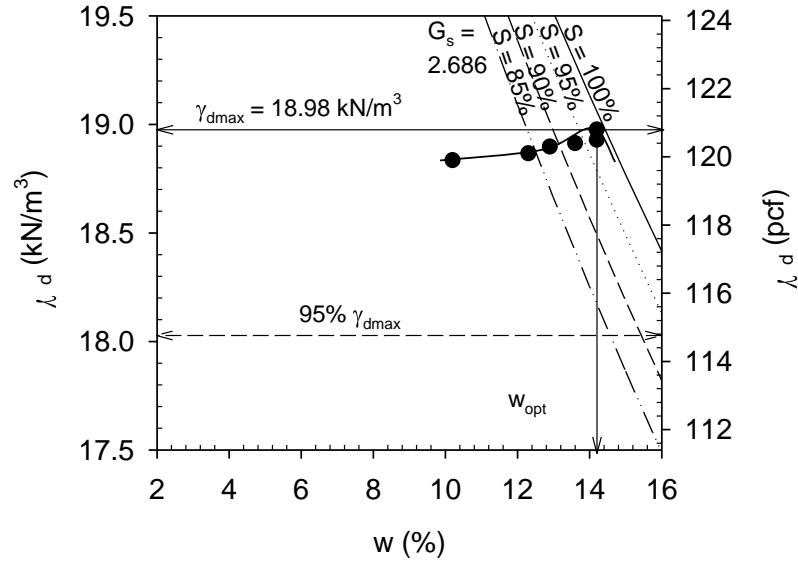
Figure 9. Results of laboratory standard Proctor test on granular embankment fill material

Experimental Test Results

TB1 Granular Embankment Fill Calibration Test Strips (Smooth Drum Roller)

TB1 consisted of granular embankment fill material placed with motor scraper and bladed with a motor grader. The test bed area was divided into two roller lanes as shown in Figure 10. Compaction was performed using the smooth drum IC roller using four roller passes. All roller passes were performed in forward motion only. Lane 1 was compacted in low amplitude mode ($a = 0.90$ mm and $f = 30$ Hz) whereas lane 2 was compacted in high amplitude mode ($a = 1.80$ mm and $f = 30$ Hz). A summary of nominal machine settings is provided in Table 2.

In-situ point-MVs (γ_d, w, DCP-CBR, and E_{LWD-Z3}) were obtained at 5 locations along lanes 1 and 2 after 0, 1, 2, and 4 roller passes. The moisture content of the subgrade material varied between 3.3% and 5.0% which is about -9 to -11% of AASHTO T-99 w_{opt}. Comparison of in-situ w and γ_d point-MVs obtained from each lane after the final roller pass with laboratory Proctor test results is shown in Figure 11. The relative compaction values in-situ varied from about 92% to 97% of standard Proctor maximum dry unit weight (AASHTO T-99 γ_{dmax}) with an average of about 94% on lane 1 and 95% on lane 2.

The objectives of testing on this test bed were to evaluate the influence of vibration amplitude on soil compaction properties (i.e., density, modulus, and CBR) and MDP* IC-MVs, and obtain comparison measurements for correlations between MDP* IC-MVs and point-MVs.

Figure 10. TB1 granular embankment fill calibration test strips
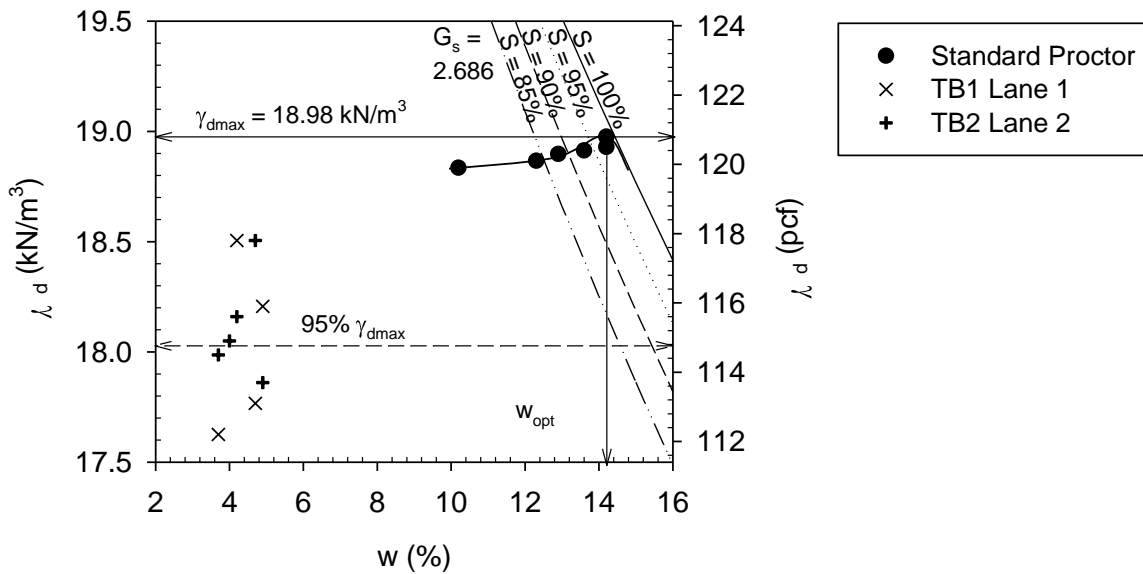
Figure 11. Comparison of in-situ moisture-dry unit weight measurements on TB1 (lanes 1 and 2 after final compaction pass) with laboratory Proctor test results

Spatial MDP* IC-MV maps for each roller pass on lanes 1 and 2 are provided in Figure 12. MDP* plots with distance are provided in Figure 13 which indicate that the values are repeatable along the test strip lane. On average, MDP* on lanes 1 and 2 generally increased with increasing number of passes, with exception of last pass on lane one which showed a decrease in the average MDP* indicating de-compaction (Figure 14). No significant differences are noticeable between the average MDP* measurements obtained using different amplitude settings on lanes 1 and 2.

Average point-MV compaction curves for lanes 1 and 2 are presented in Figure 14. On average, E_{LWD-Z3} and DCP-CBR decreased from pass 0 to 1 and then increased up to pass 4. On the other hand, γ_d almost remained unchanged with increasing pass. MDP* IC-MV plots (as lines) in comparison with point-MVs (as points) along lane 1 after passes 1, 2, and 4 are presented in Figure 15 and Figure 16. Similarly, plots from lane 2 are presented in Figure 17 and Figure 18. Regression analysis results between IC-MVs and point-MVs by spatially pairing the nearest point data is presented in the Regression Analysis section later in this report.
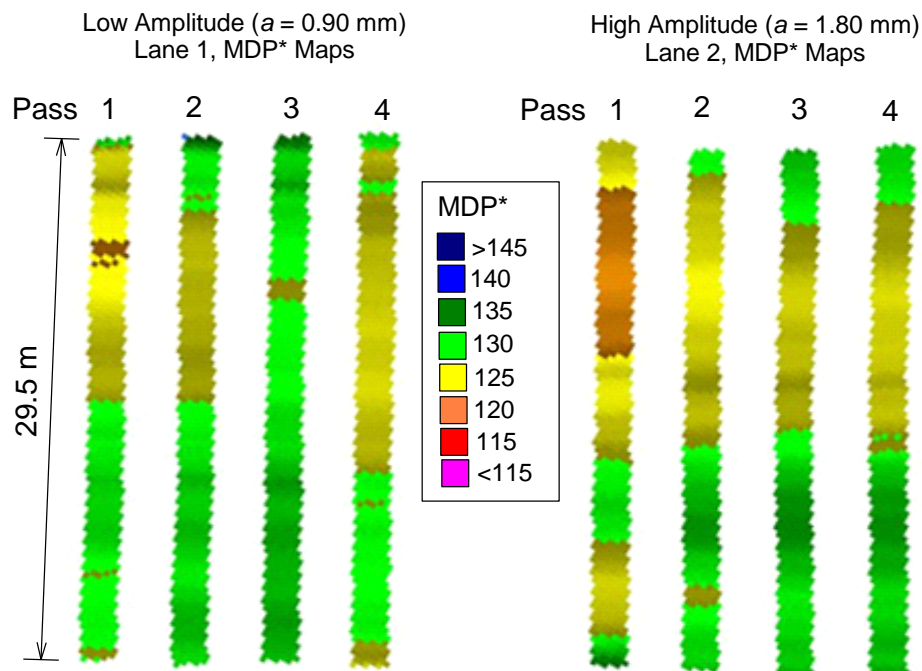
Figure 12. MDP* maps on lanes 1 and 2 – TB1 granular embankment fill
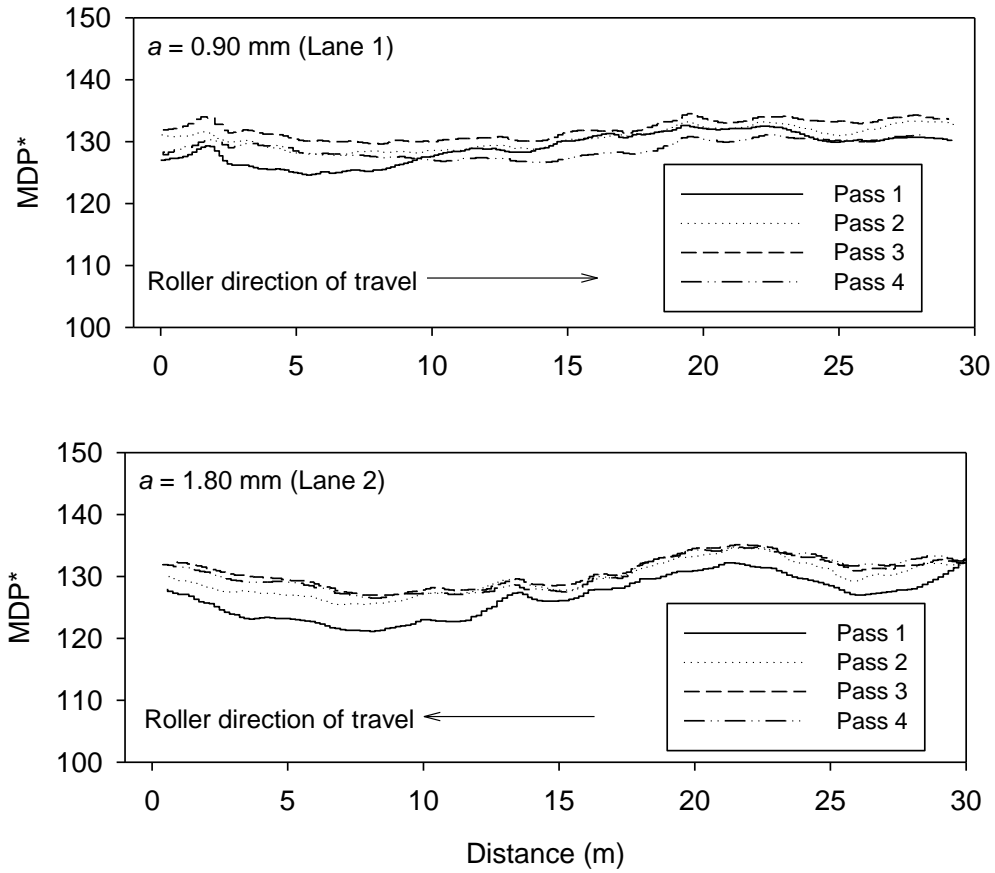
Figure 13. MDP* linear plots on lanes 1 and 2 – TB1 granular embankment fill
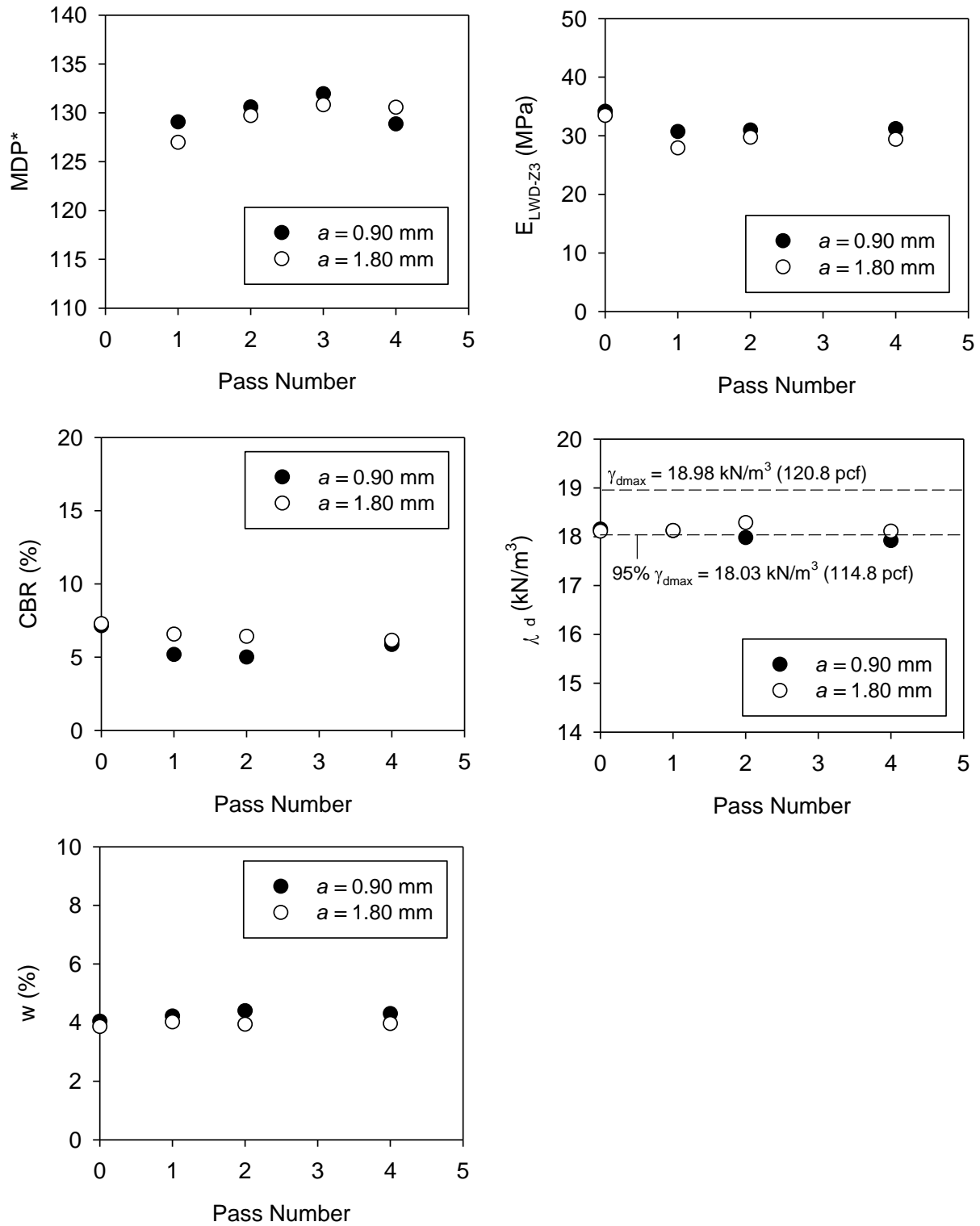
Figure 14. MDP* and in-situ point-MV compaction curves lane 1 (*a* = 0.90 mm) and lane 2 (*a* = 1.80 mm) – TB1 granular embankment fill
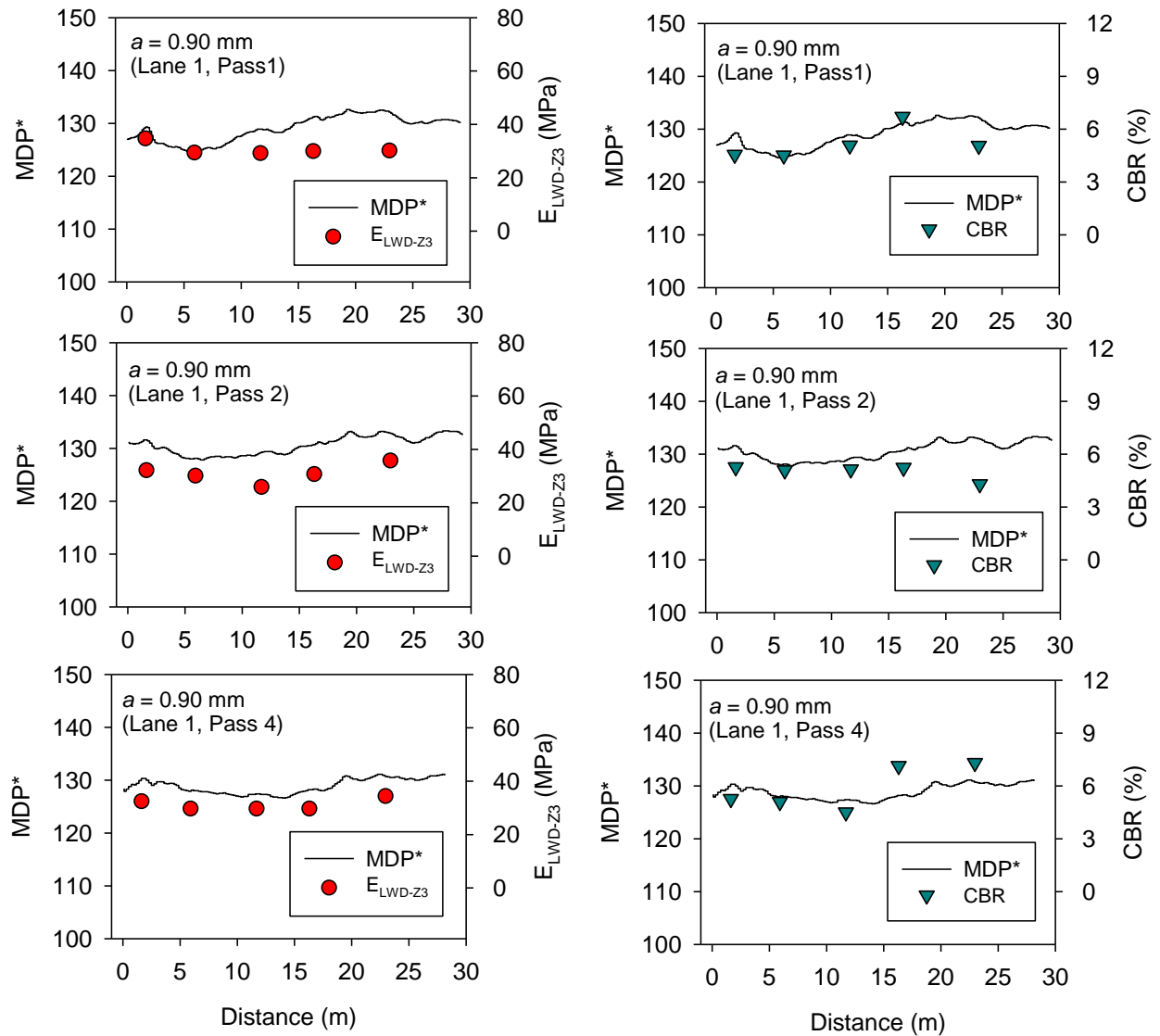
Figure 15. Comparison between MDP* and in-situ point-MVs (E_{LWD-Z3} and CBR) on lane 1 (a = 0.90 mm) – TB1 granular embankment fill
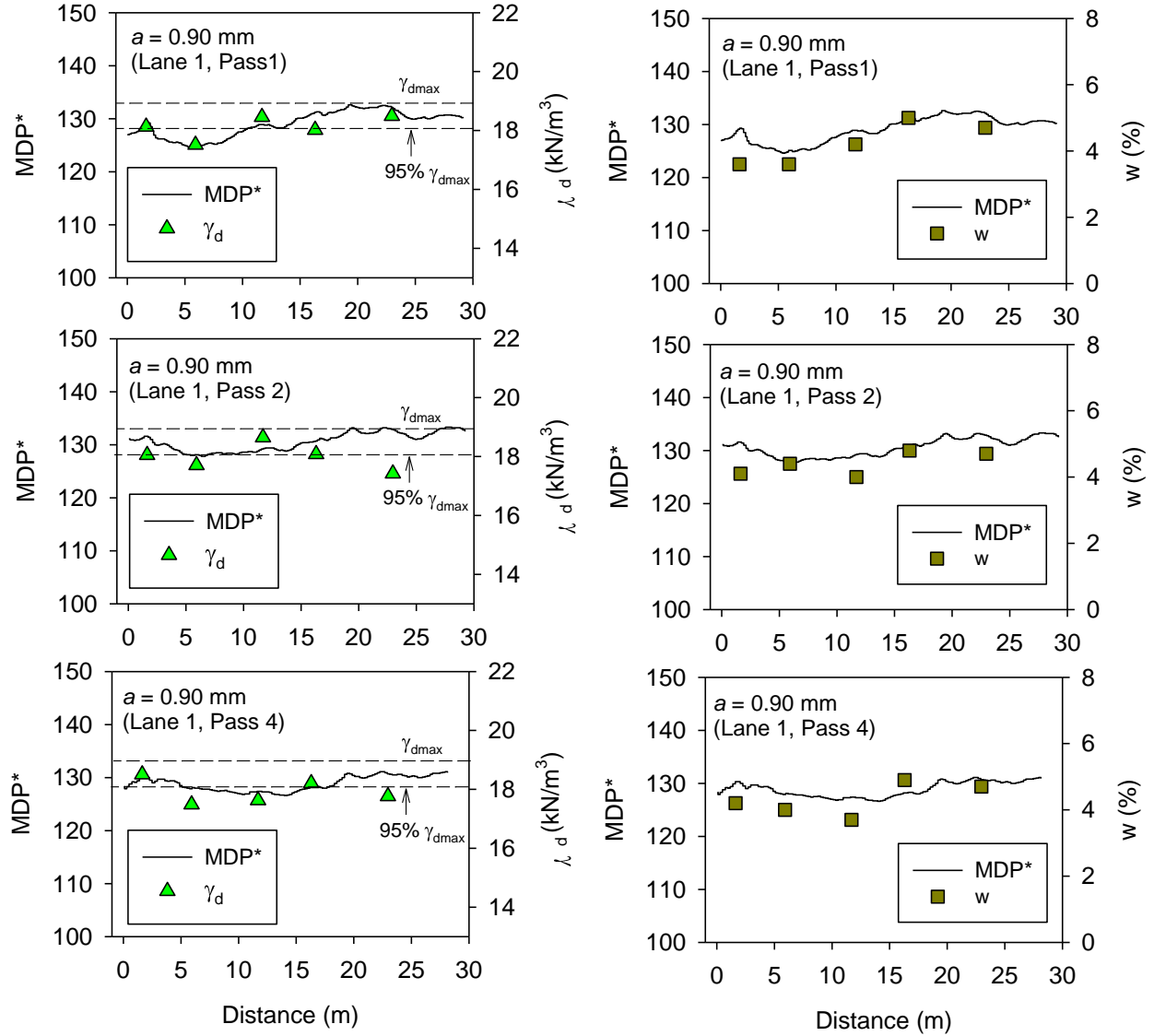
Figure 16. Comparison between MDP* and in-situ point-MVs (γ_d and w) on lane 1 (a = 0.90 mm) – TB1 granular embankment fill
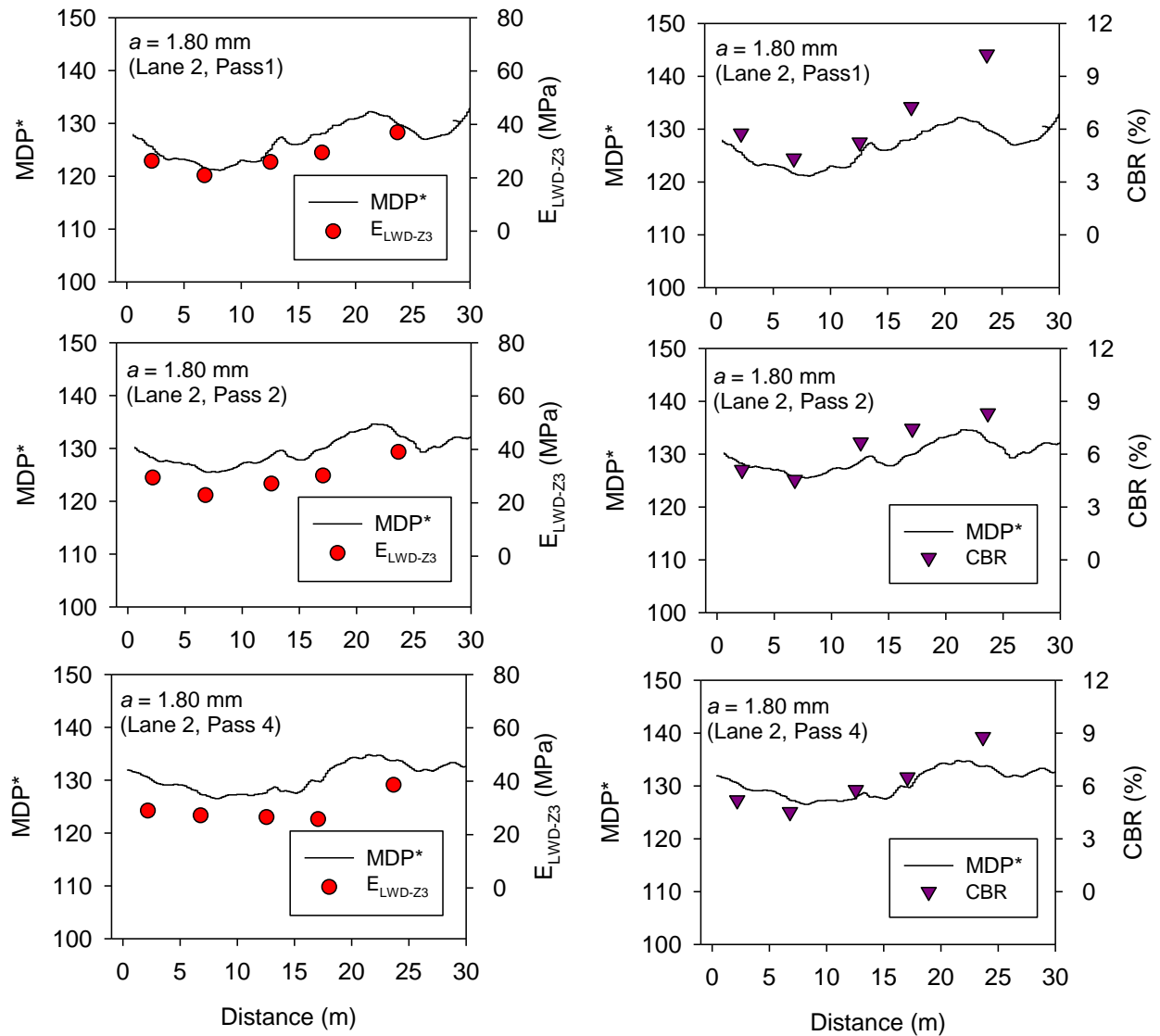
Figure 17. Comparison between MDP* and in-situ point-MVs (E_{LWD-Z3} and CBR) on lane 2 ($a = 1.80$ mm) – TB1 granular embankment fill
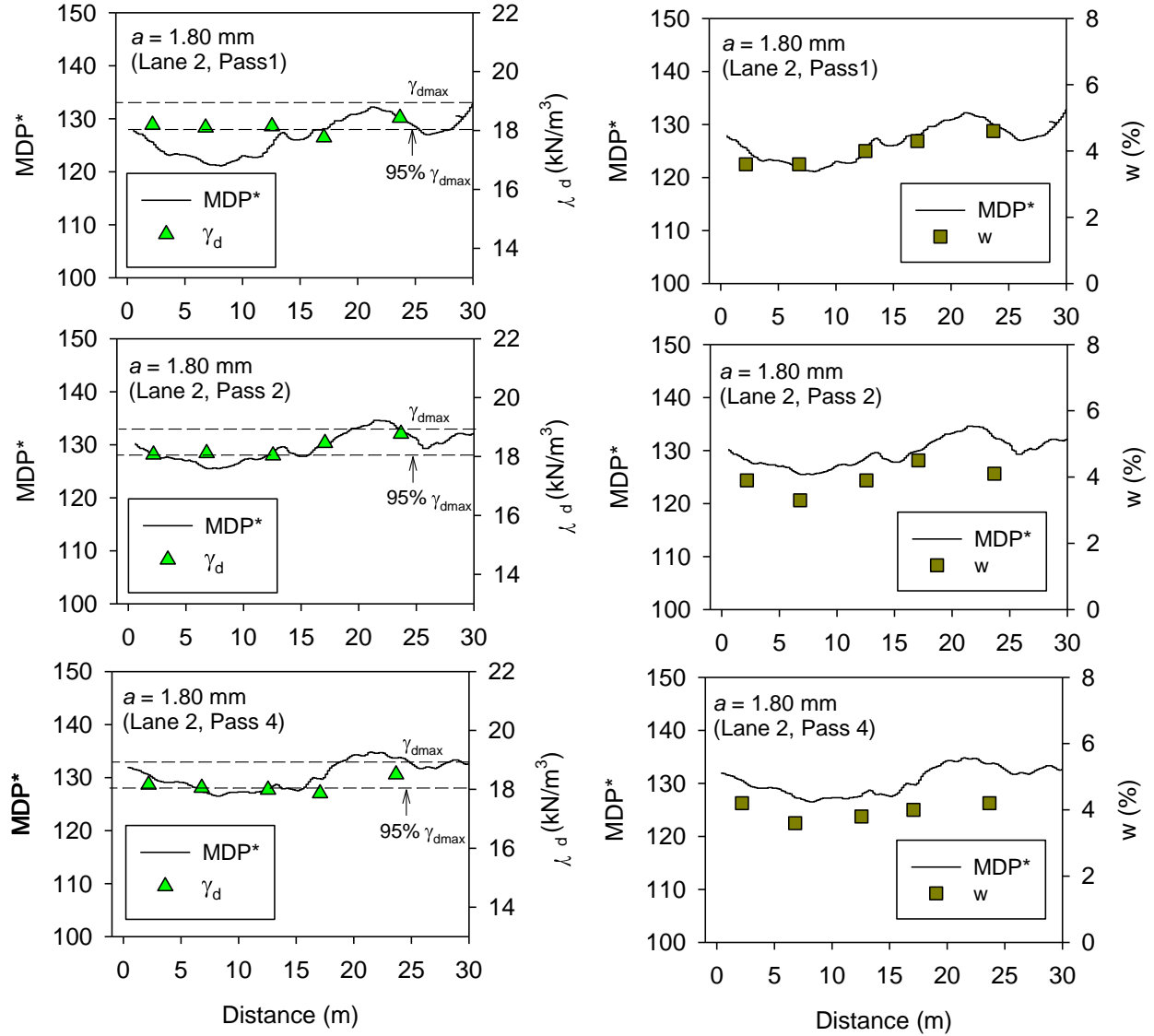
Figure 18. Comparison between MDP* and in-situ point-MVs (γ_d and w) on lane 2 ($a = 1.80$ mm) – TB1 granular embankment fill

20

TB2 Sandy Embankment Fill Calibration Test Strip (Smooth Drum Roller)

TB2 consisted of granular embankment fill material. Compaction was performed using the smooth drum IC roller using sixteen passes with eight in forward gear and eight in reverse gear. All passes were made in low amplitude mode ($a = 0.90$ mm and $f = 30$ Hz). A summary of nominal machine settings is provided in Table 2. The main objective of obtaining sixteen passes was to assess how repeatable and reproducible the measurements are in forward and reverse motions. After the final roller pass, LWD tests were conducted at one location at multiple depths, i.e., at 0, 42 mm (1.7 in), 125 mm (4.9 in), 210 mm (8.3 in), 300 mm (11.8 in), and 362 mm (14.3 in) below the surface (Figure 19). The main objective of conducting LWD testing at multiple depths was to assess the influence of confinement on LWD modulus values.

MDP* IC-MV results from forward and reverse passes are presented in Figure 20. Average MDP* values with increasing pass number are presented in Figure 21. These results indicate that the MDP* values are repeatable in both forward and reverse passes. Reproducible analysis showed some differences due to operating conditions. For example, within 2 to 10 m range, MDP* values range between 125 to 149 in forward gear while the values range between 125 to 138 in reverse gear. Further, on average the values in forward gear are about 2% higher than in reverse gear. Average MDP* results presented with increasing pass presented in Figure 21 indicate that there is no consistent increase in MDP* with pass due to de-compaction of the material (as indicated by a reduction in the average MDP* for passes 5, 8, 13, and 15 in forward gear and for passes 6, 9, 12, and 14 in reverse gear)

Figure 19. LWD testing at multiple depths on TB2 – Granular embankment fill
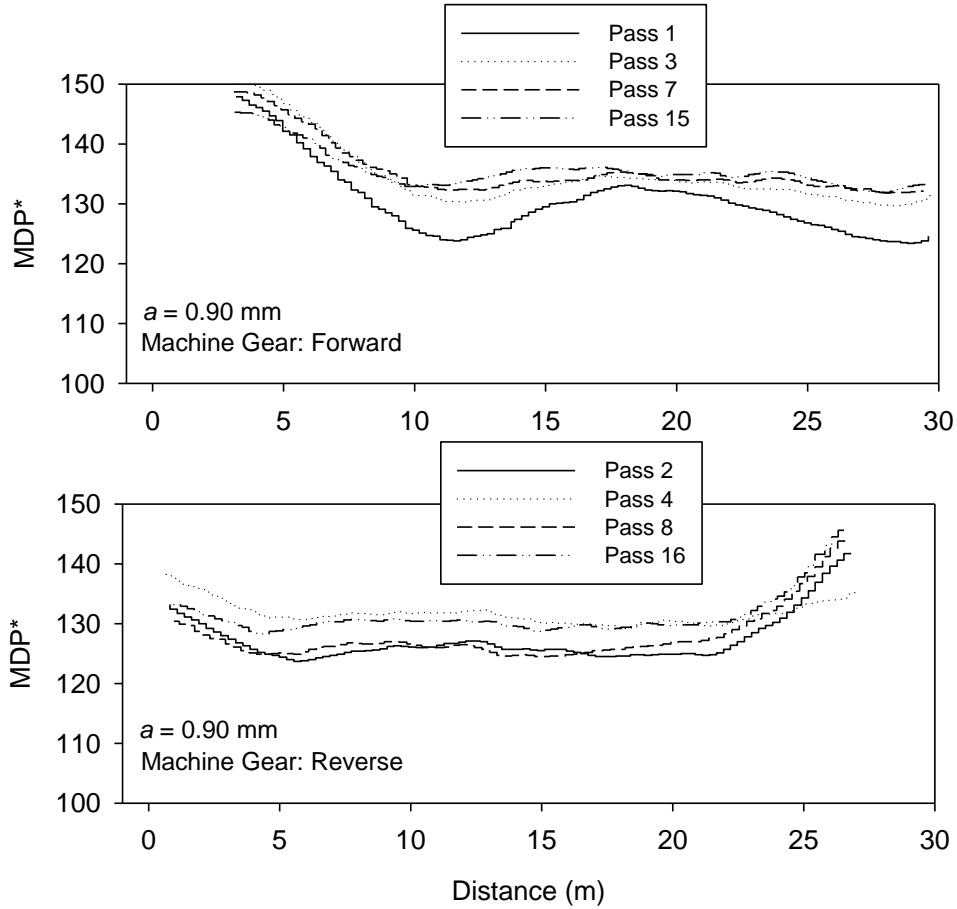
Figure 20. MDP* data for multiple roller passes in forward and reverse machine gear – TB2 granular embankment fill
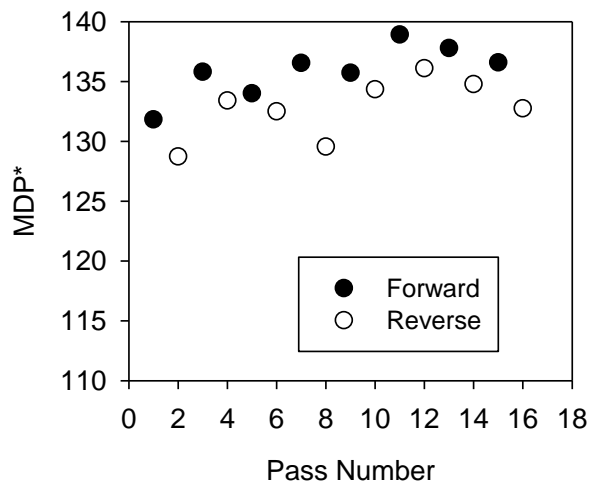
Figure 21. Average MDP* with increasing roller passes in forward and reverse gears – TB2 granular embankment fill

Results from LWD tests conducted at multiple depths are presented in Figure 22. These results indicate that the E_{LWD-Z3} measurements generally increase with depth as a result of increasing confinement. This is of consequence and important to understand as it affects the determined "target values" during calibration testing. Lambe and Whitman (1969) indicated that as confining pressure (σ_c) increases elastic modulus increases by σ_c^n where n varies from 0.4 to 1.0. Figure 22 shows a trend line illustrating the influence of confinement on E_{LWD-Z3} values neglecting any potential influence of relative density, moisture, or gradation changes with depth and is expressed as Eq. 6, where $E_{LWD-Z3(d)} = E_{LWD-Z3}$ value at depth d, $E_{LWD-Z3(s)} = E_{LWD}$ at surface, λ and n = regression factors.

$$E_{LWD-Z3(d)} = \lambda \left[E_{LWD-Z(3)(s)} (d) \right]^n \tag{6}$$

The results indicate that E_{LWD-Z3} values increase by about 150% at a depth of about 150 mm. A similar finding was presented by White et al. (2009a) based on testing performed on several project sites with granular soils in Minnesota, but with a different trend line as shown in Figure 22.
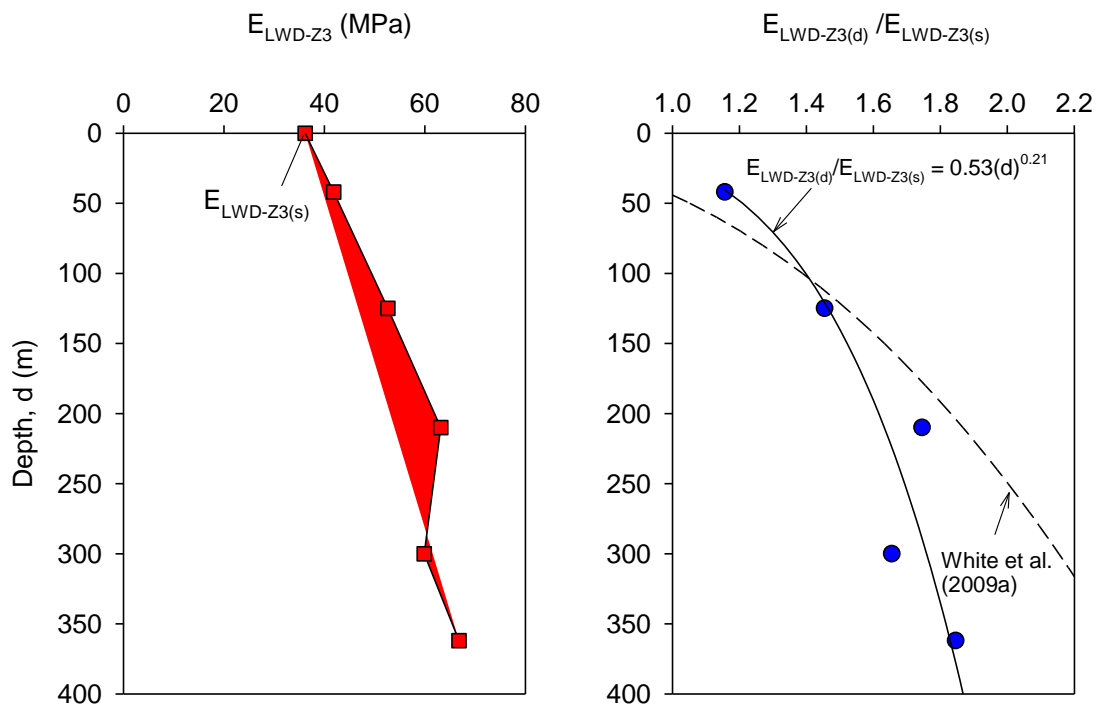
Figure 22. LWD tests at different depths illustrating the influence of confinement on in-situ soil modulus – TB2 granular embankment fill

23

TB4 Silty Clay Subgrade Calibration Test Strips (Padfoot Roller)

TB4 consisted of cohesive embankment fill material (Figure 23). The test bed area was divided into two roller lanes. Compaction was performed using the padfoot IC roller using eight roller passes. All roller passes were performed in forward motion only. Lane 1 was compacted in low amplitude mode ($a = 0.90$ mm and $f = 30$ Hz) whereas lane 2 was compacted in static mode. A summary of nominal machine settings is provided in Table 2.

In-situ point-MVs (γ_d, w, DCP-CBR, and $E_{LWD\text{-}Z3}$) were obtained at 7 locations along lanes 1 and 2 after the final roller pass. The moisture content of the subgrade material varied between 8.2% and 17.1% which is about -9.1 to -0.1% of AASHTO T-99 w_{opt}, with an average of about 13.5% (-3.7% of w_{opt}). Comparison of in-situ w and γ_d point-MVs obtained from each lane with laboratory Proctor test results is shown in Figure 24. The relative compaction values in-situ varied from about 98% to 108% of AASHTO T-99 γ_{dmax} with an average of about 102% on lane 1 and 105% on lane 2.

The objectives of testing on this test bed were to evaluate the influence of vibration amplitude on compaction properties (i.e., density, modulus, and CBR) of cohesive soils and MDP* IC-MVs, and obtain comparison measurements for correlations between MDP* IC-MVs and point-MVs.

Spatial MDP* IC-MV maps for each roller pass on lanes 1 and 2 are provided in Figure 25. MDP* plots with distance are provided in Figure 26 which indicate that the values are repeatable along the test strip lane. On average, MDP* on lane 2 compacted in static mode increased with increasing number of passes up to pass 7 and then decreased slightly (from MDP* = 96.1 to 94.0) (Figure 27). On the other hand, average MDP* on lane 1 compacted in low amplitude mode showed an inconsistent trend during passes 2 and 5 that is attributed to off-tracking. On average, MDP* values after pass 8 were about the same on both lanes. Average point-MVs before compaction and after pass 8 are presented in Figure 27. Results indicate that on average, $E_{LWD\text{-}Z3}$, DCP-CBR, and γ_d values on lane 2 compacted in static mode were about 1.5, 1.03, and 1.3 times, respectively higher compared to the values on lane 1 compacted in low amplitude mode. The reason for lower values on lane 1 is attributed to possible surface disturbance under vibration.

MDP* IC-MV plots (as lines) in comparison with point-MVs (as points) along lanes 1 and 2 after pass 8 are presented in Figure 28 and Figure 29, respectively. Regression analysis results between IC-MVs and point-MVs by spatially pairing the nearest point data is presented in the Regression Analysis section later in this report.

Figure 23. Construction of TB4 silty clay subgrade calibration test strips
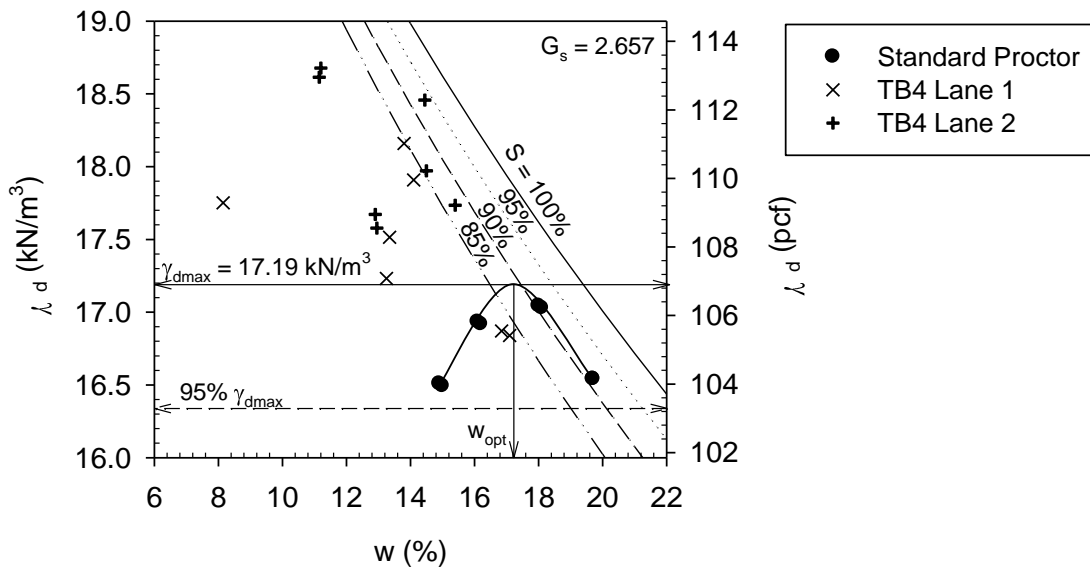
Figure 24. Comparison of in-situ moisture-dry unit weight measurements on TB3 (lanes 1 and 2 after final compaction pass) with laboratory Proctor test results
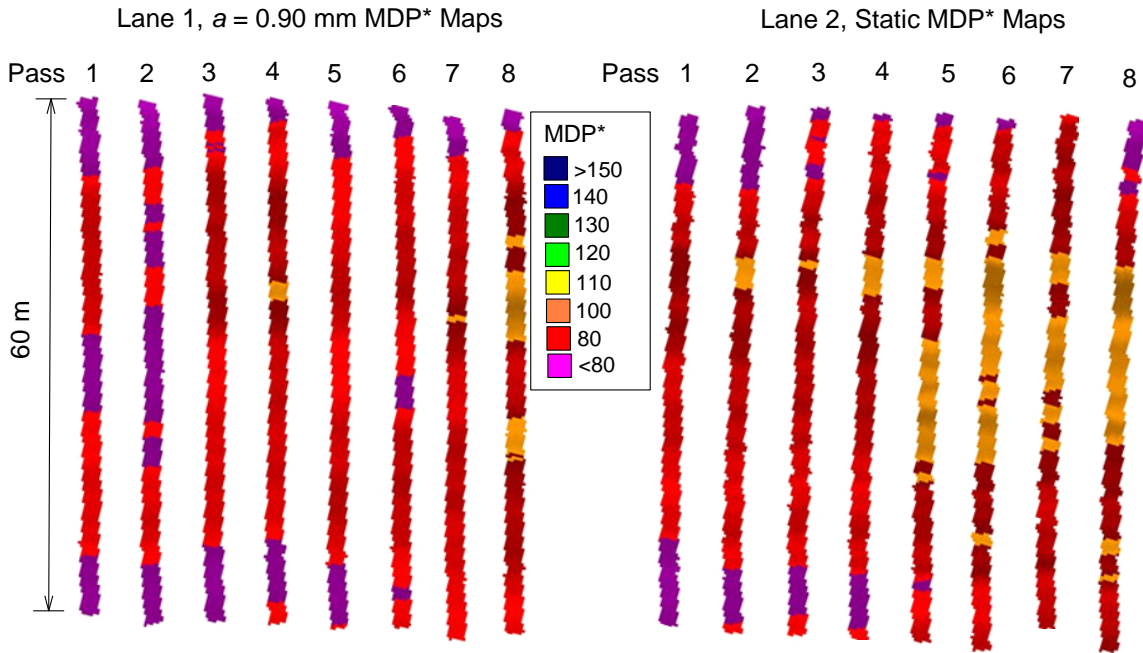
Figure 25. MDP* maps from passes 1 to 8 on lanes 1 and 2 – TB4 silty clay subgrade
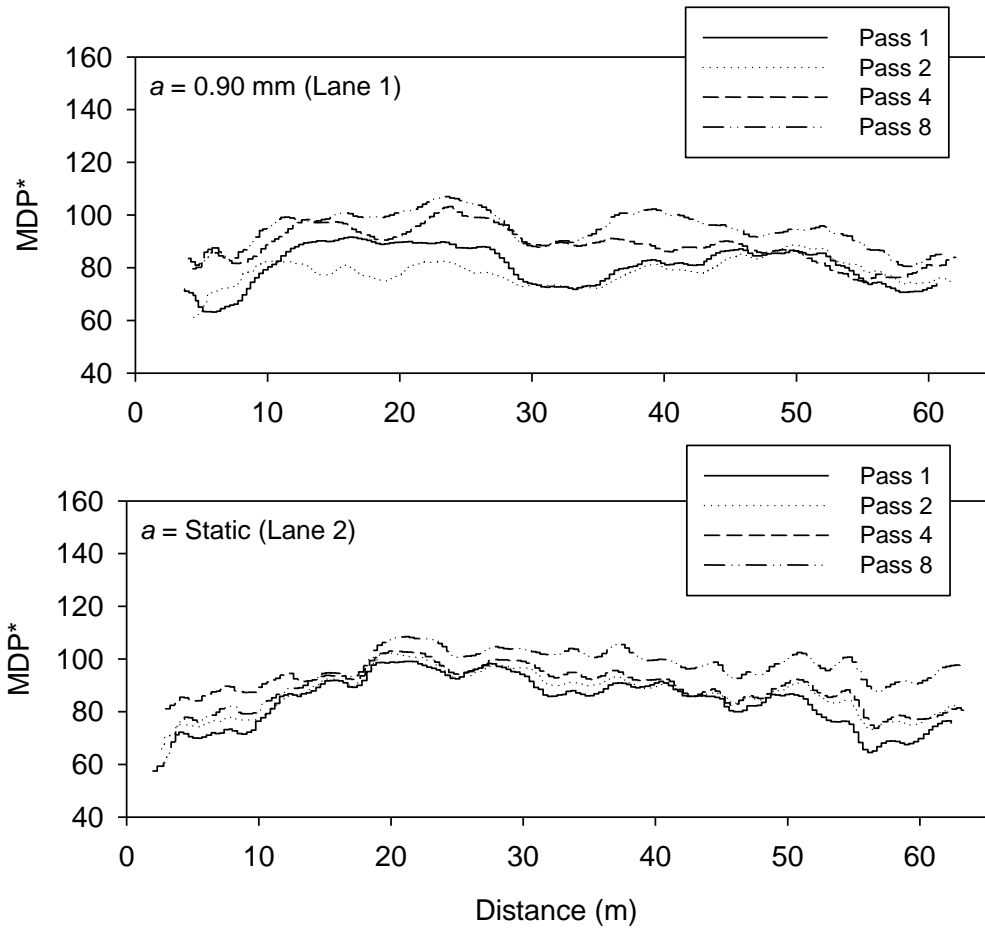
Figure 26. MDP* linear plots on lanes 1 and 2 – TB4 silty clay subgrade calibration strips
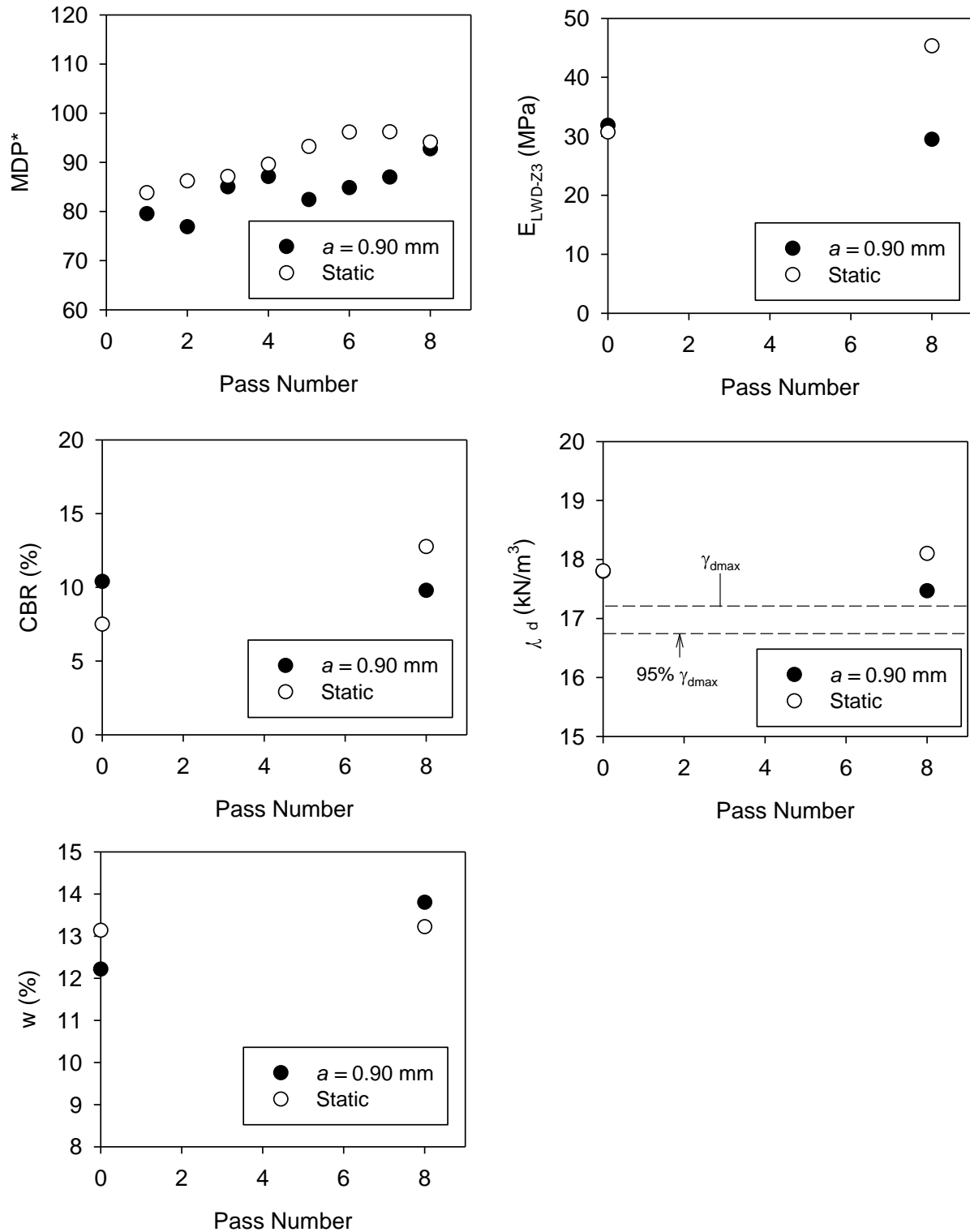
Figure 27. MDP* and in-situ point-MV compaction curves lane 1 (*a* = 0.90 mm) and lane 2 (static) – TB4 silty clay subgrade calibration strips
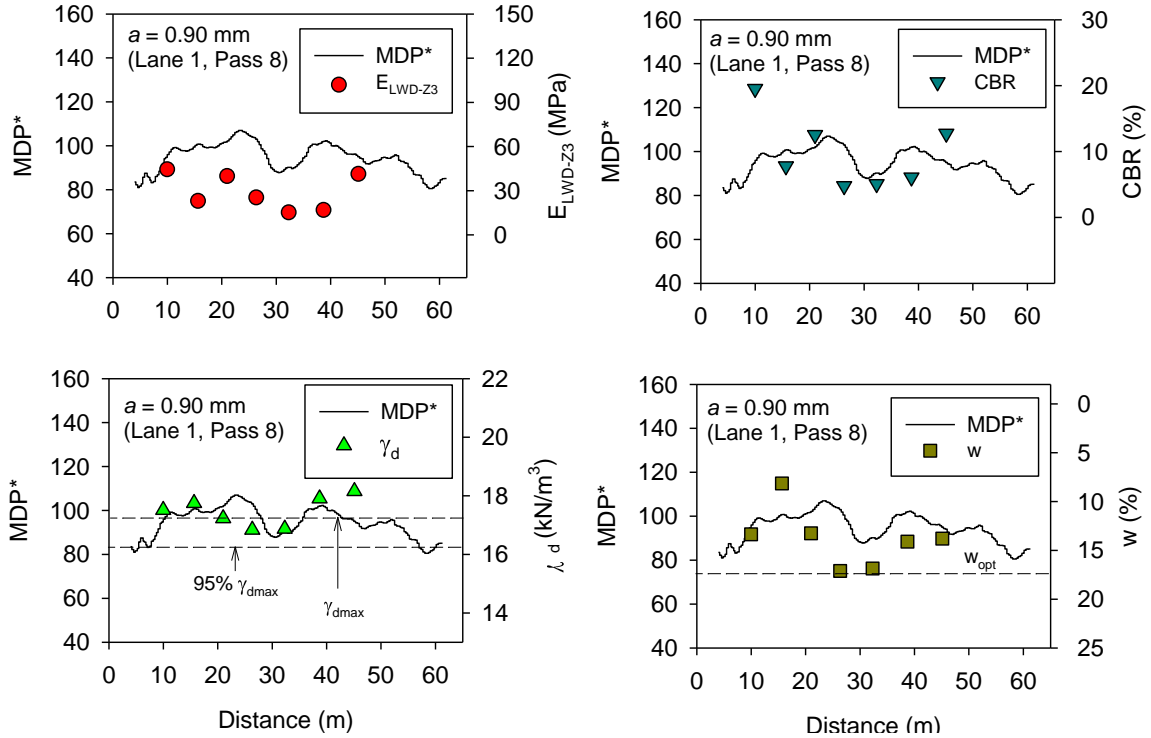
Figure 28. Comparison between MDP* and in-situ point-MVs on lane 1 (*a* = 0.90 mm) – TB4 silty clay subgrade calibration strips
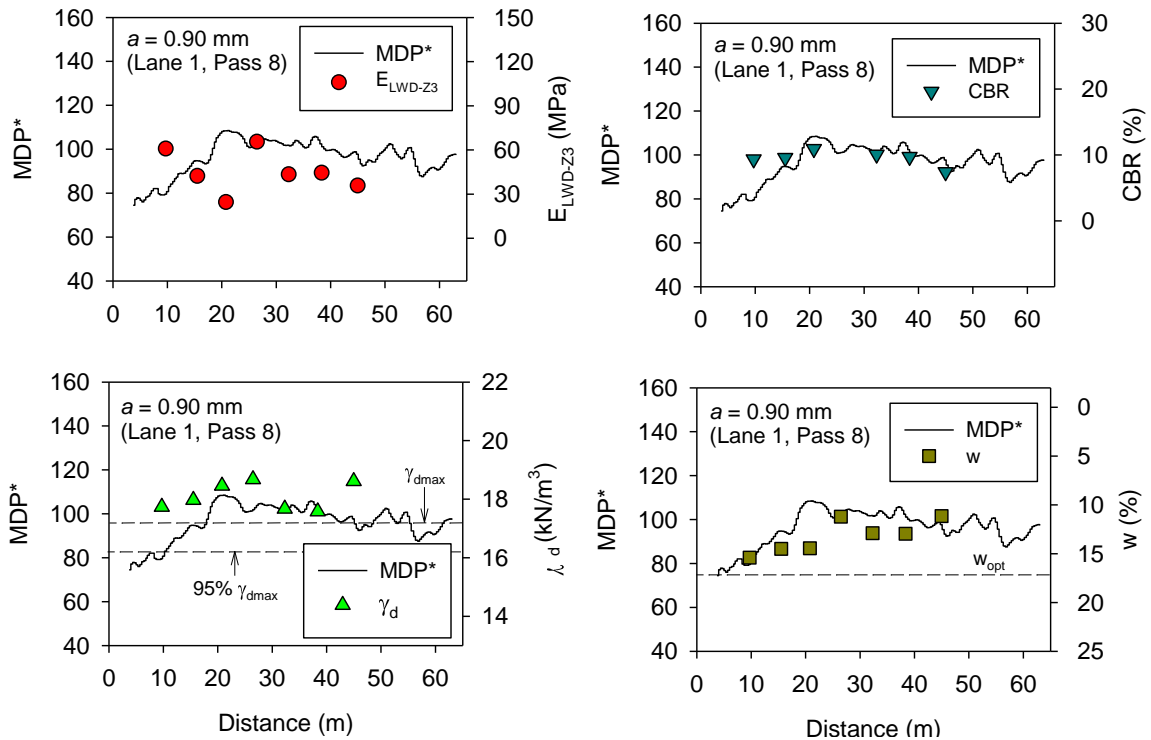
Figure 29. Comparison between MDP* and in-situ point-MVs on lane 1 (*a* = 0.90 mm) – TB4 silty clay subgrade calibration strips

TB5 Cohesive Embankment Fill Test Strip (Padfoot Roller)

TB5 consisted of a 48 m long test strip with compacted cohesive embankment fill material and was located adjacent to TB4. The test bed visually showed rutting or sinkage under construction traffic loading and was selected to evaluate variable ground conditions (Figure 30). The test bed area was mapped using one roller pass in low amplitude setting ($a = 0.90$ mm and $f = 30$ Hz) and using eight passes in static mode using the padfoot IC roller. The MDP* values varied from about 65 to 145 along the test strip. Following the final roller pass, E_{LWD-Z3} point-MVs were obtained at 72 locations along the test strip at relative dense point-point spacing (~0.65 m (2 ft)). MDP* IC-MVs in comparison with E_{LWD-Z3} point-MVs are presented in Figure 31. Both MDP* and E_{LWD-Zs} measurements tracked well on this test strip. Regression analysis results between IC-MVs and point-MVs by spatially pairing the nearest point data is presented in the Regression Analysis section later in this report.

Figure 30. TB5 cohesive embankment fill test strip
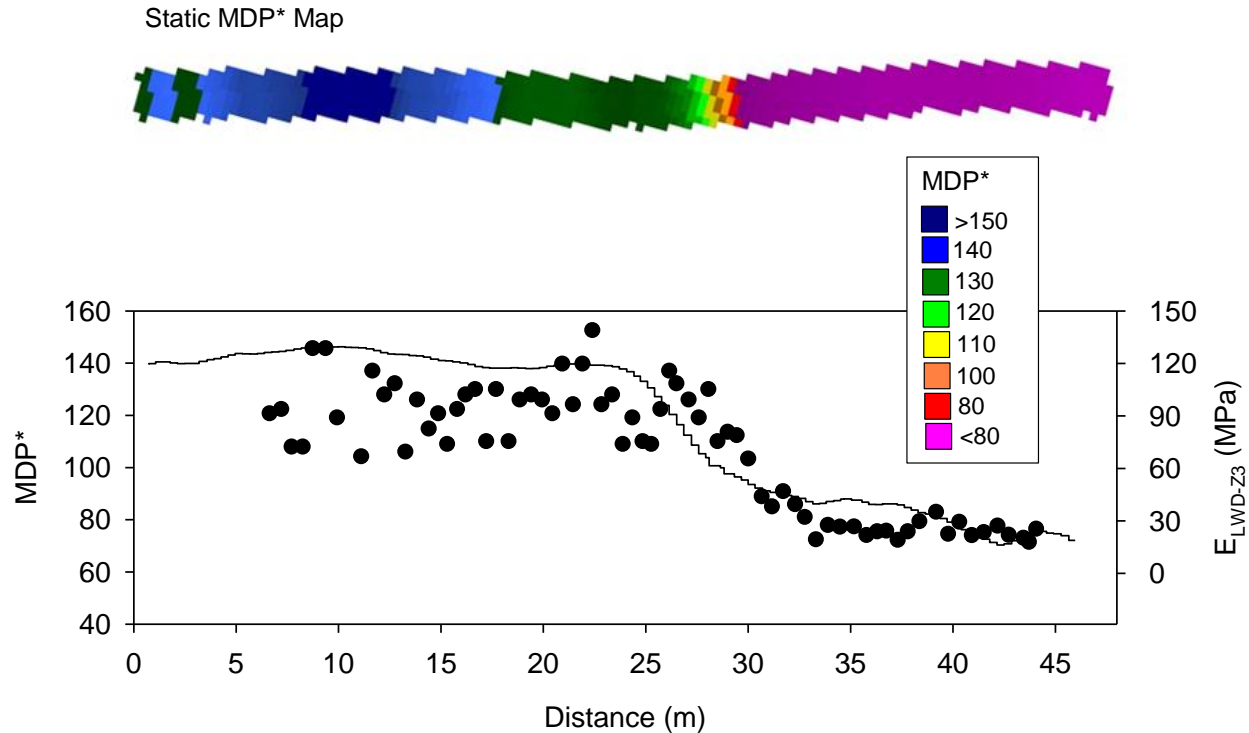
Figure 31. Comparison between MDP* and E$_{LWD-Z3}$ – TB5 silty subgrade test strip

TBs 3 and 6 Granular Embankment Fill Production Area (Smooth Drum Roller)

Test Bed Construction and In-Situ Test Results

This test bed consisted of a production area with granular embankment fill with two lifts (Lift # 1 – TB3 and Lift # 2 – TB6) (Figure 32). Lift 1 was mapped using two roller passes and E$_{LWD-Z3}$ testing was performed in a selected area with high, medium and low IC-MVs using the on-board display. Tests were performed at 20 locations with relatively high IC-MVs, 16 locations with medium range IC-MVs, and 28 test locations with relatively low IC-MVs. DCP tests were also performed at 7 selected locations. After compaction and testing on lift # 1, lift # 2 (TB6) was placed and compacted using four roller passes in low amplitude mode (*a* = 0.90 mm and *f* = 30 Hz). Nominal machine settings during each pass are summarized in Table 2. Compaction operations on lift # 2 were performed by the contractor. The roller operator was trained on-site to make use of the on-board display unit and was instructed to perform four roller passes over the production area. After the final pass, E$_{LWD-Z3}$ testing was performed at 42 test locations across the production area. Test locations were selected based on the IC display to capture high, medium, and low values. In addition, DCP and NG tests were also performed at 7 selected locations.

Spatial MDP* maps from TB3-lift # 1 for the two passes are presented in Figure 33. MDP* plots with distance along each roller lane in comparison with E$_{LWD-Z3}$ measurements on lift # 1 are presented in Figure 33. DCP-CBR profiles obtained from seven test locations are presented in Figure 34. As expected, DCP-CBR profiles showed that CBR generally increases with depth due to the confinement effect as discussed earlier in this report. Spatial MDP* and roller pass

30

coverage maps from TB6-lift # 2 for the four passes are presented in Figure 36. MDP* plots with distance along each roller lane in comparison with E_{LWD-Z3} measurements on lift # 2 are presented in Figure 37. DCP-CBR profiles obtained from eight test locations are presented in Figure 38. In-situ w and γ_d results from NG tests are shown in Figure 38. The moisture content of the fill material varied from about 3.5% to 5.1% which is about -9 to -11% of AASHTO T-99 w_{opt}, and the relative compaction of the fill material varied from about 95% to 110% with an average of about 97% of AASHTO T-99 γ_{dmax}.

The E_{LWD-Z3} values generally tracked well with variations in the MDP* values on both lifts # 1 and 2, except at some locations on lanes 2 and 6 on lift # 1. Regression analysis results between IC-MVs and point-MVs by spatially pairing the nearest point data is presented in the Regression Analysis section later in this report.

Figure 32. TB6 granular embankment fill production area lift # 2
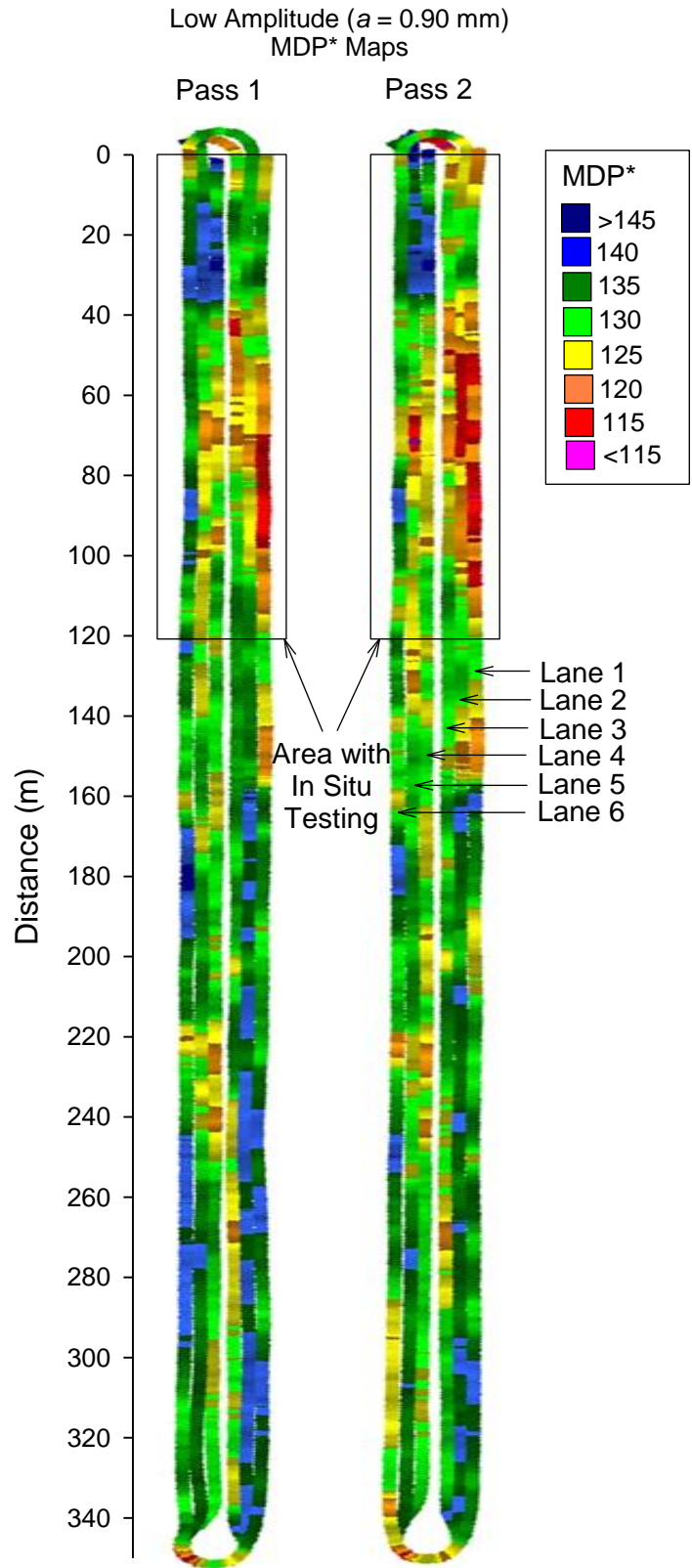
Figure 33. MDP* maps – TB3 granular embankment fill production area lift # 1
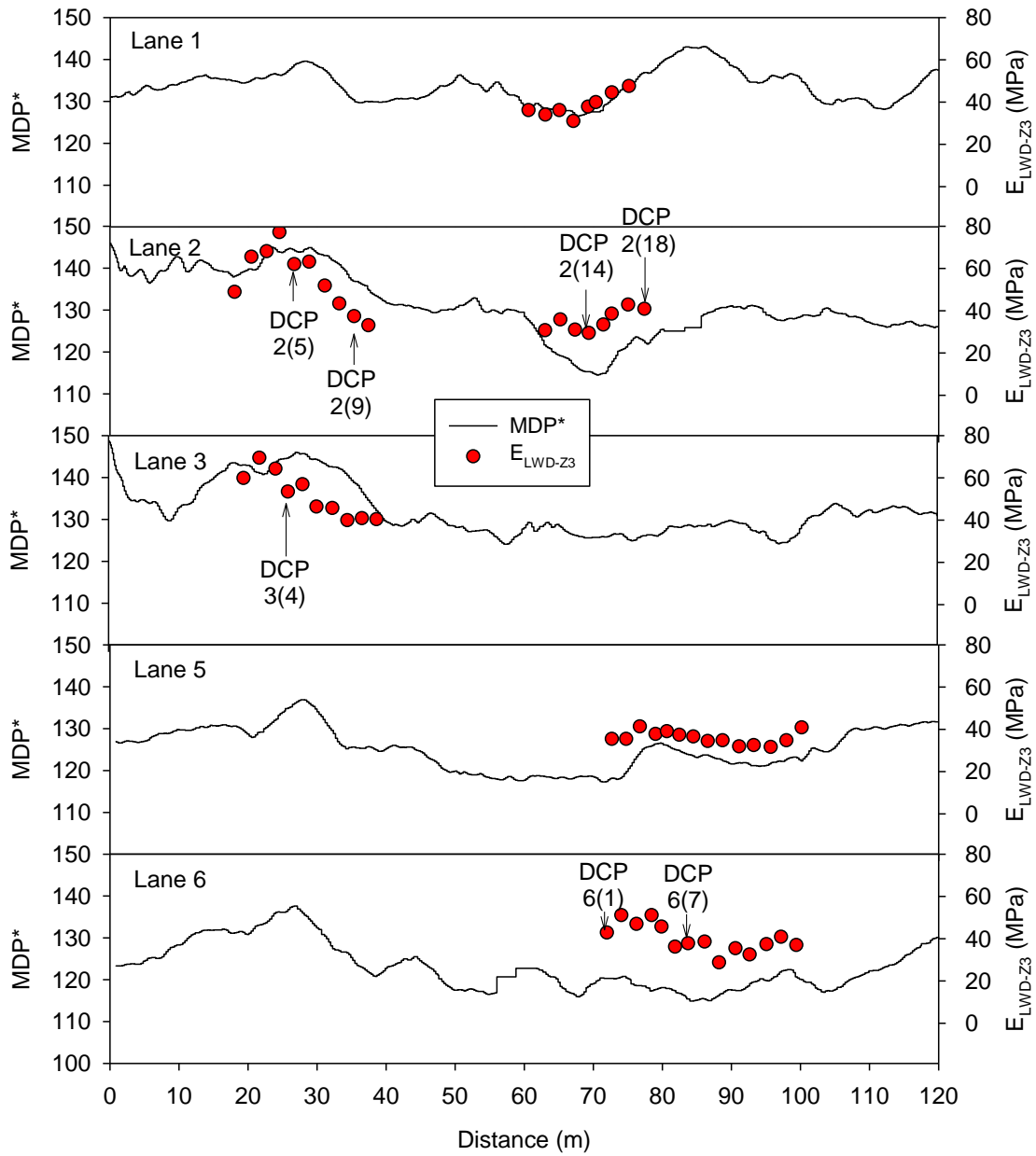
Figure 34. Comparison between MDP* and E$_{LWD-Z3}$ point-MVs from different lanes – TB3 granular embankment fill production area lift # 1
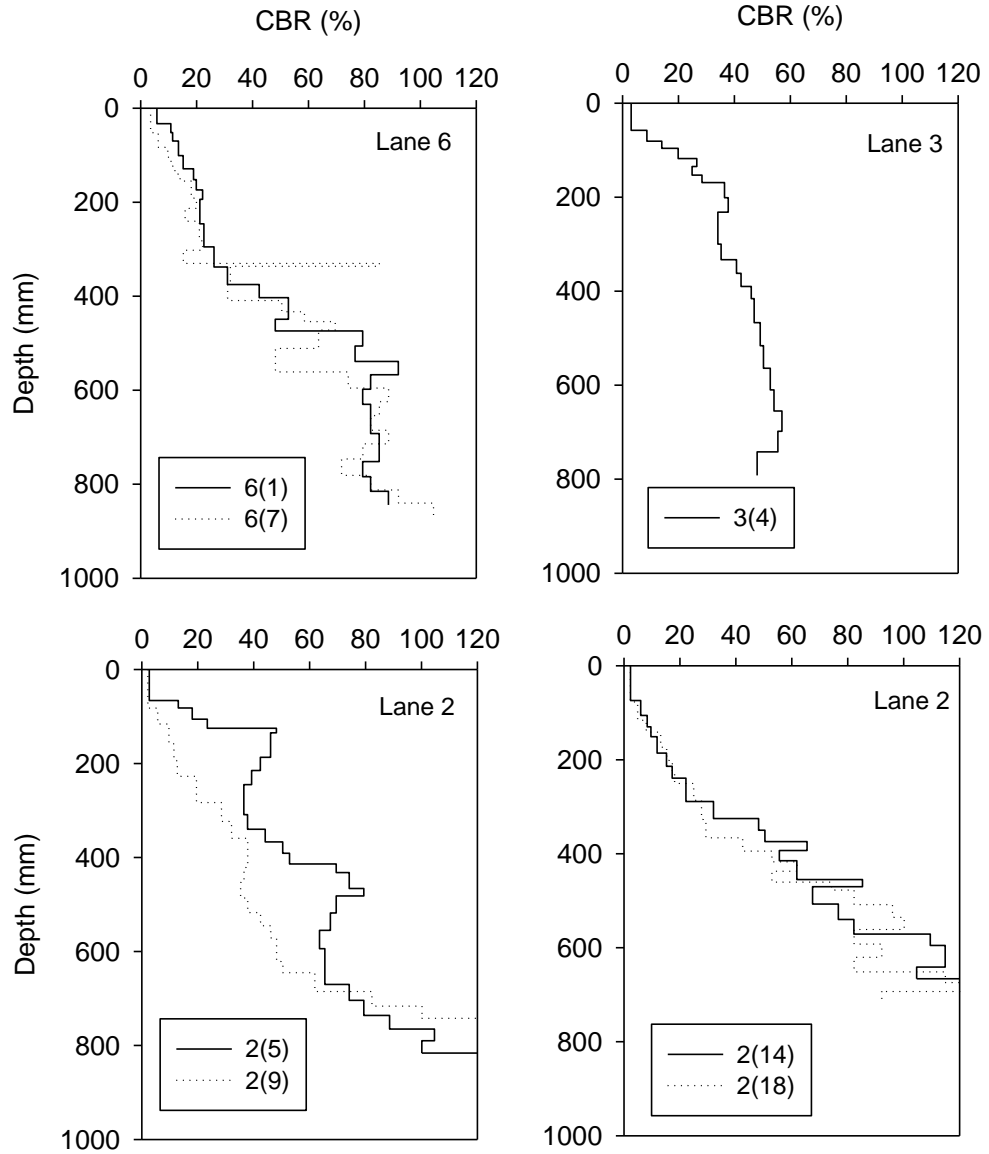
Figure 35. DCP-CBR profiles from different lanes – TB3 granular embankment fill production area lift # 1 (Note: 6(1) indicates roller lane number 6 and test location number 1)

34
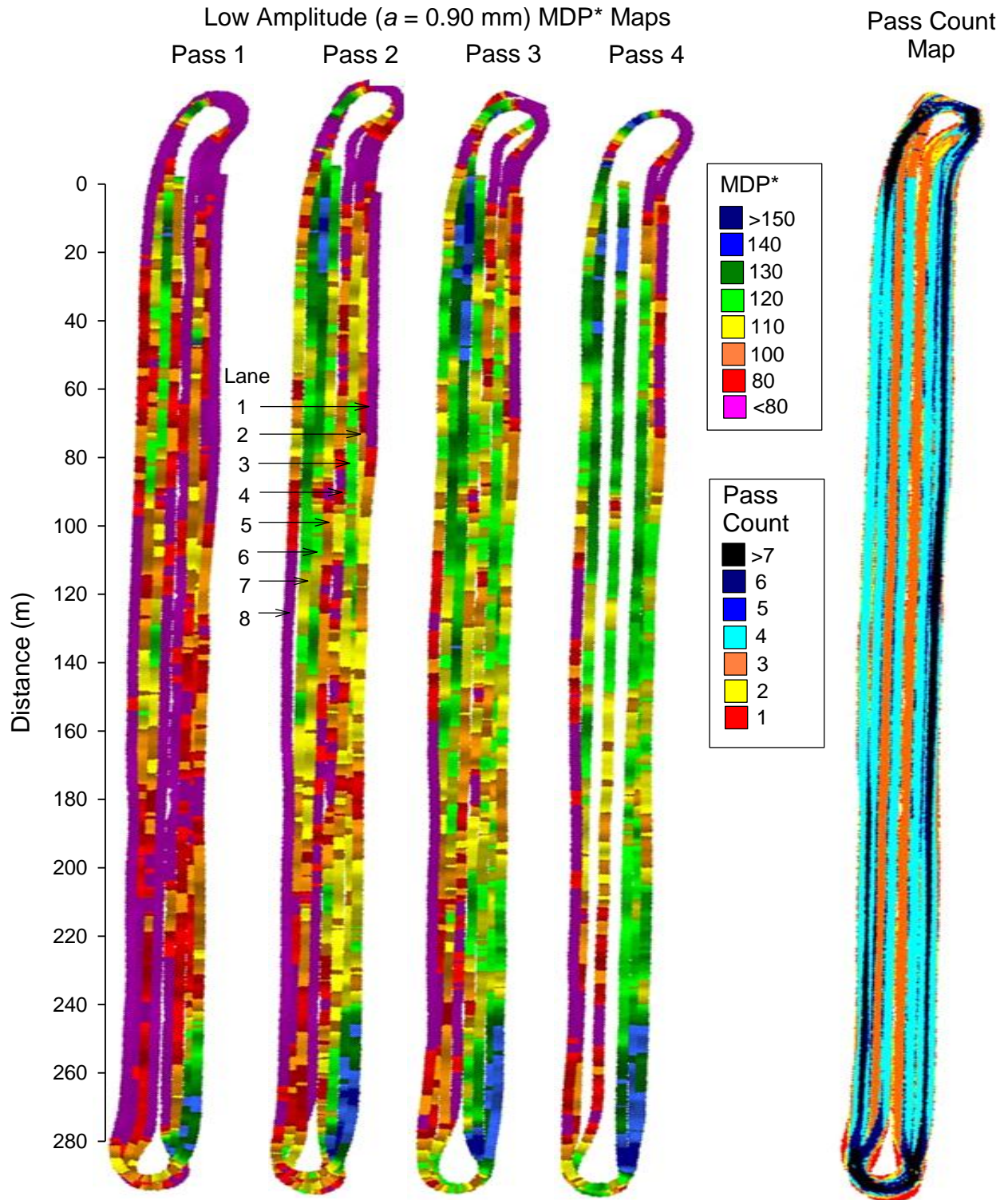
**Figure 36. MDP* and pass count maps – TB6 granular embankment fill production area lift # 2**
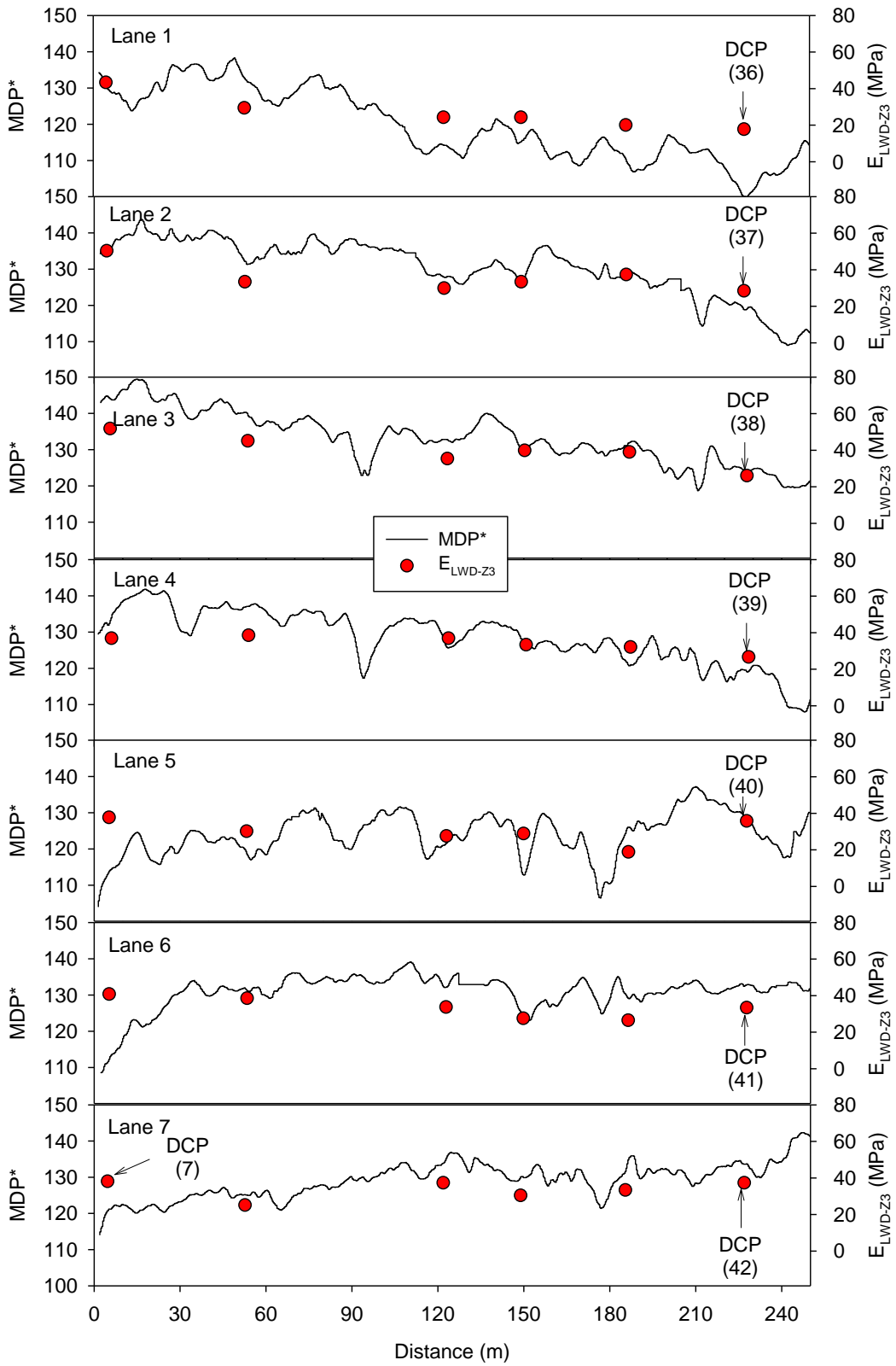
Figure 37. Comparison between MDP* and E$_{LWD-Z3}$ point-MVs from different lanes – TB6 granular embankment fill production area lift # 2

(36) γ_d = 17.99 kN/m^3, w = 4.0   (40) γ_d = 18.90 kN/m^3, w = 4.2

(37) γ_d = 18.46 kN/m^3, w = 3.4   (41) γ_d = 18.21 kN/m^3, w = 4.3

(38) γ_d = 18.90 kN/m^3, w = 3.7   (42) γ_d = 18.28 kN/m^3, w = 5.1

(39) γ_d = 18.79 kN/m^3, w = 3.8
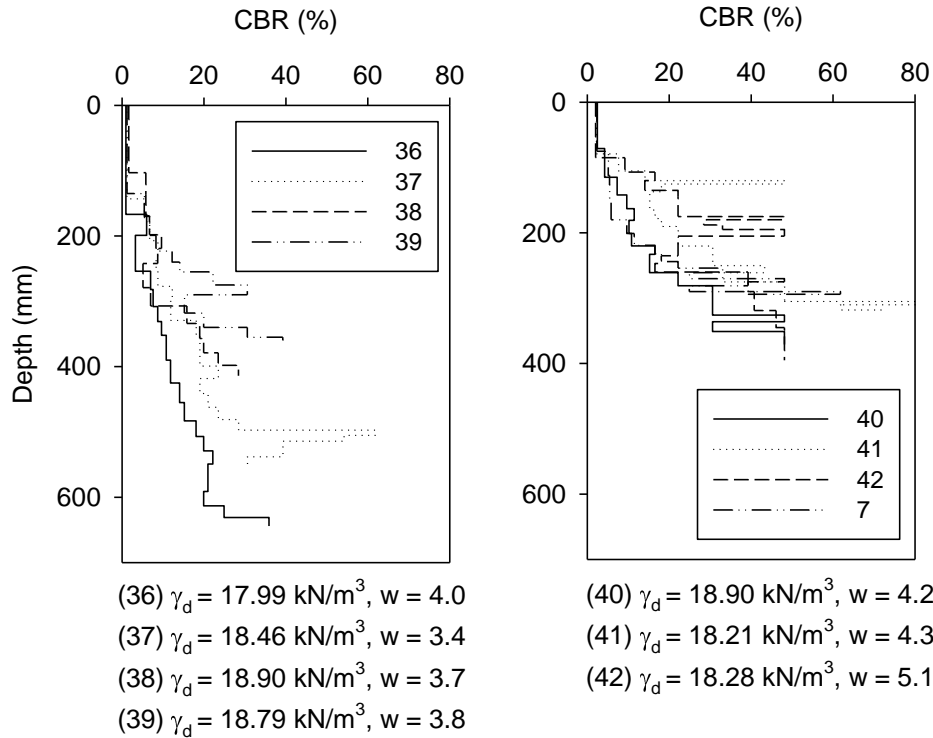
Figure 38. DCP-CBR profiles from different lanes – TB6 granular embankment fill production area lift # 2

Geostatistical Analysis

Figure 39 shows MDP* histogram plots for the two passes on lift # 1 (TB3) along with a summary of univariate statistics (i.e., mean μ, standard deviation σ, coefficient of variation COV). Geostatistical semivariograms of MDP* for the two passes are also shown in Figure 39, with a summary of spatial statistics (i.e., nugget, sill, and range). The experimental semivariograms values showed a nested spatial structure with short-range and long-range components. Nested spherical variograms were fit to the experimental semivariogram data. It is possible that the long-range spatial structure is linked to the spatial variation in underlying layer support conditions while the short-range spatial structure is a result of soil properties close to the surface. Similar nested variograms were observed in a previous field study conducted in New York and North Dakota as part of the FHWA IC pooled fund study. These concepts have not previously been evaluated and could provide an important step in understanding the spatial variability associated with IC data.

Figure 40 presents MDP* histogram plots and MDP* semivariogram plots for the four passes on lift # 2 (TB6) along with a summary of univariate and spatial statistics. Theoretical spherical variograms are fit to the experimental variogram data. The spatial and univariate statistics indicate that variability in MDP* measurements increased slightly from pass 1 to 2 and then decreased for pass 3 (as evidenced by change in sill values and standard deviation values). No considerable change in variability was noticed between passes 3 and 4 MDP* data. The average

37

MDP*, however, increased with increasing pass. Comparison between MDP* semivariograms from lift s # 1 and 2 indicate that the MDP* measurements on lift # 2 were more variable as evidenced by comparatively high sill values than on lift # 1. Interestingly, the Geostatistical range values were similar on both lifts (i.e., about 9 to 10 m). Nested structures were not observed on lift # 2 as observed on lift # 1.
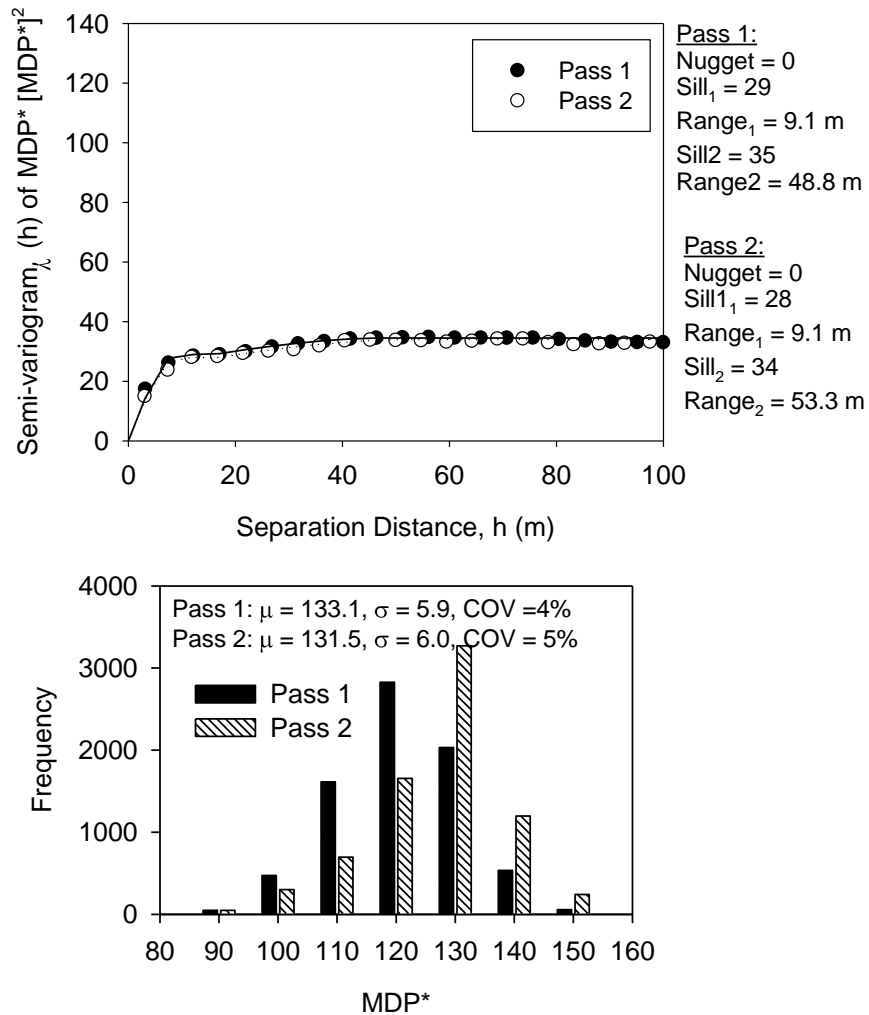
Figure 39. Geostatistical semi-variograms and histograms of passes 1 and 2 on lift # 1 – TB 3 granular embankment fill production area
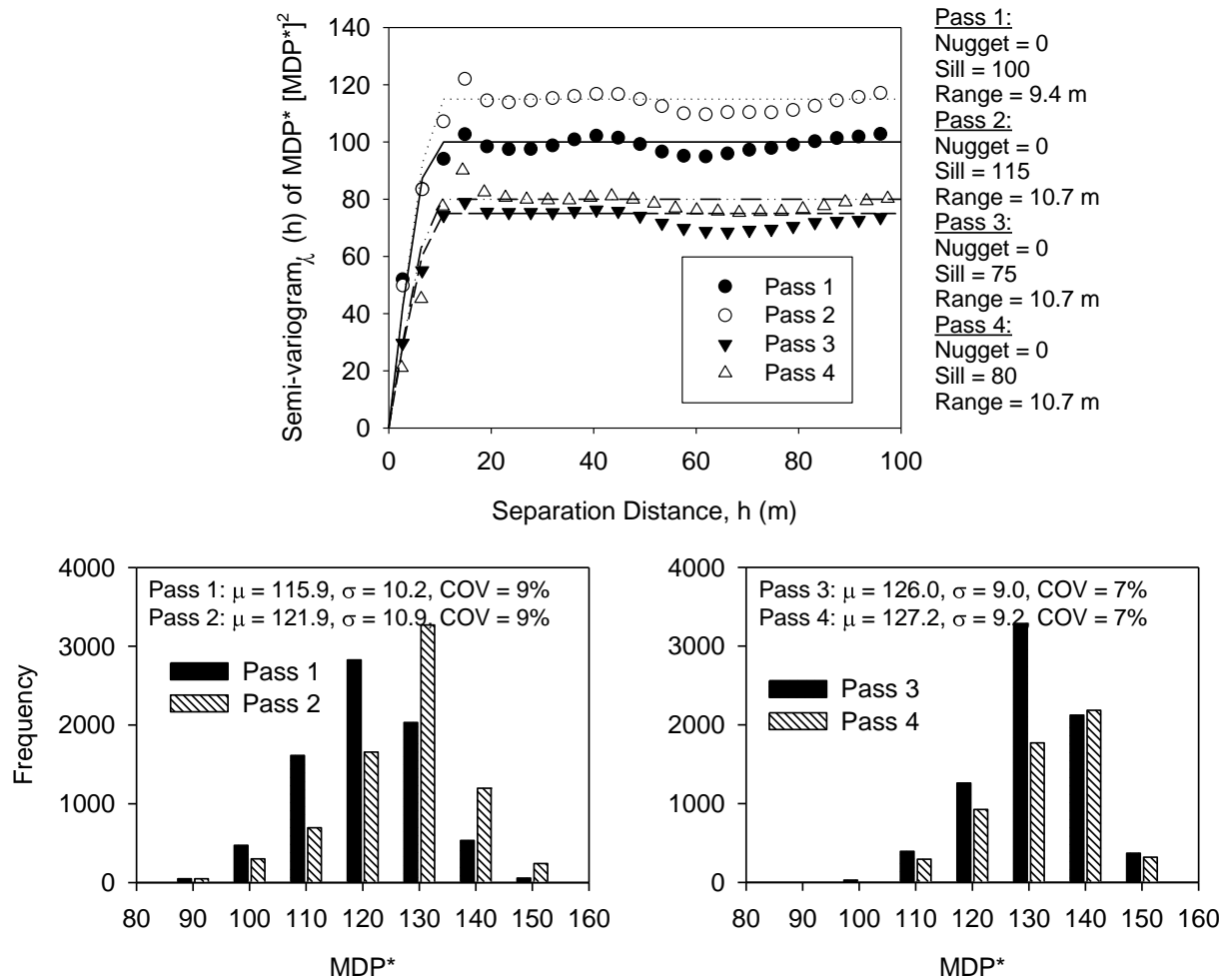
Figure 40. Geostatistical semi-variograms and histograms of passes 1 to 4 on lift # 2 – TB 6 granular embankment fill production area

Regression analysis

Data presented above captured MDP* IC-MVs and corresponding in-situ point-MVs over a wide measurement range. The data from multiple test beds (with similar machine settings) are combined in this section to develop site wide correlations.

Relationships between MDP* obtained from smooth drum roller using $a = 0.90$ mm and $f = 30$ Hz nominal settings and in-situ point-MVs based on the data obtained from TBs 1, 3, and 6 are presented in Figure 41. All the relationships showed significant scatter with R^2 values < 0.4. Comparatively, correlation between MDP* and E_{LWD-Z3} showed better relationship with $R^2 = 0.38$ compared to γ_d and DCP-CBR. Relationships between MDP* obtained from smooth drum roller using $a = 1.80$ mm and $f = 30$ Hz nominal settings and in-situ point-MVs based on the data obtained from TB1 are presented in Figure 42. Again, correlation between MDP* and E_{LWD-Z3}

showed comparatively better relationship with $R^2 = 0.72$ compared to γ_d and DCP-CBR ($R^2 = 0.21$ and 0.52).

Relationships between MDP* obtained from padfoot roller in static mode and in-situ point-MVs based on the data obtained from TBs 4 and 5 are presented in Figure 43. Correlation between MDP* and E_{LWD-Z3} showed a power relationship with $R^2 = 0.75$, while correlations with γ_d and CBR measurements did not show a statistically significant relationship. It must be noted that measurements were obtained over a wide range of MDP* measurements (75 to 140) in correlation with E_{LWD-Z3}, while the MDP* measurements ranged only within a narrow range in correlation with γ_d and CBR (80 to 110). Relationships between MDP* obtained from padfoot roller using $a = 0.90$ mm and $f = 30$ Hz nominal settings and in-situ point-MVs based on the data obtained from TB4 are presented in Figure 44. No statistically significant relationships were observed from this dataset due to limited number of measurements.
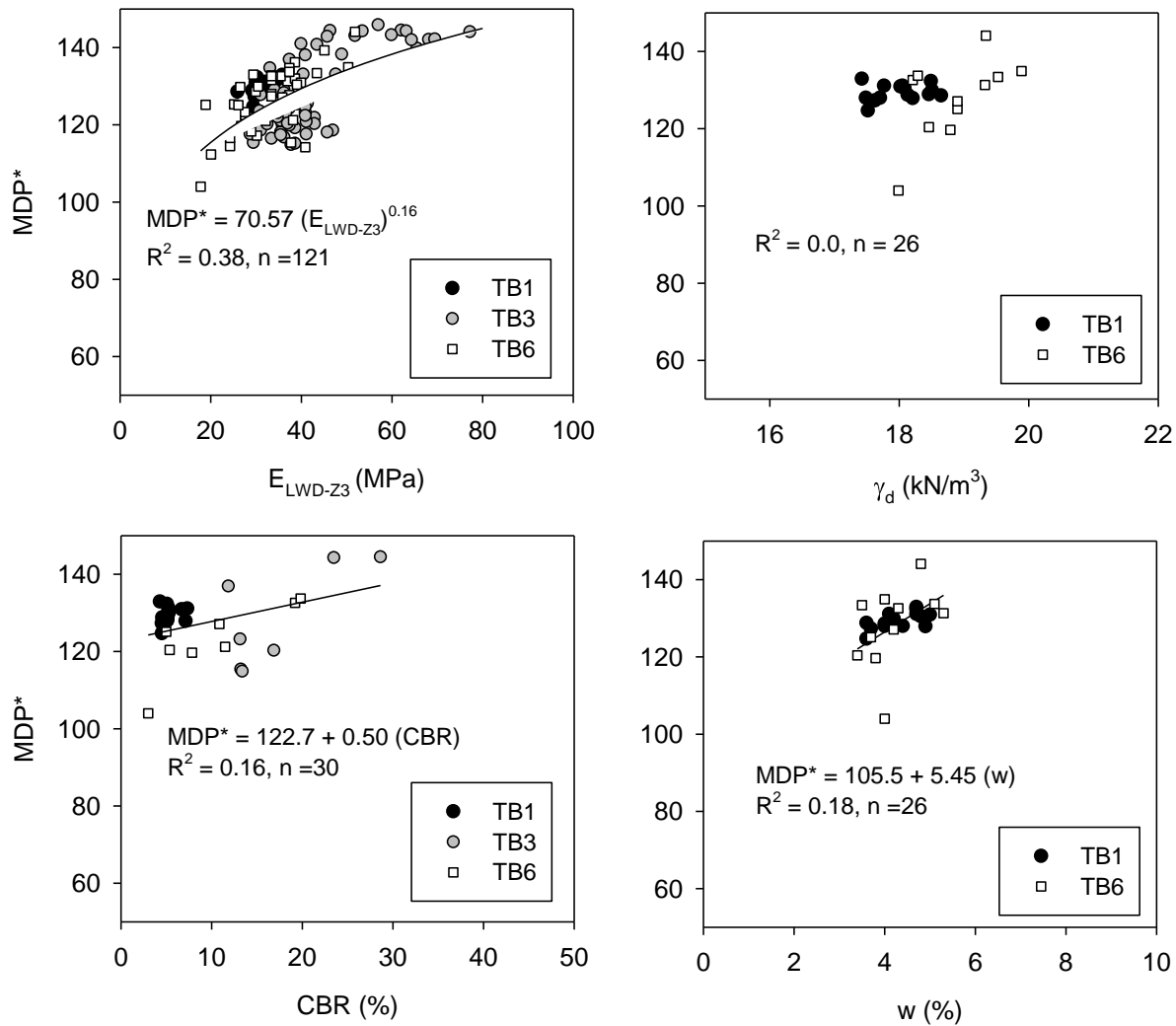
Figure 41. Correlations between MDP* and in-situ point-MVs – smooth drum roller with *a* = 0.90 mm setting (TBs 1, 3, and 6 granular embankement fill)

40
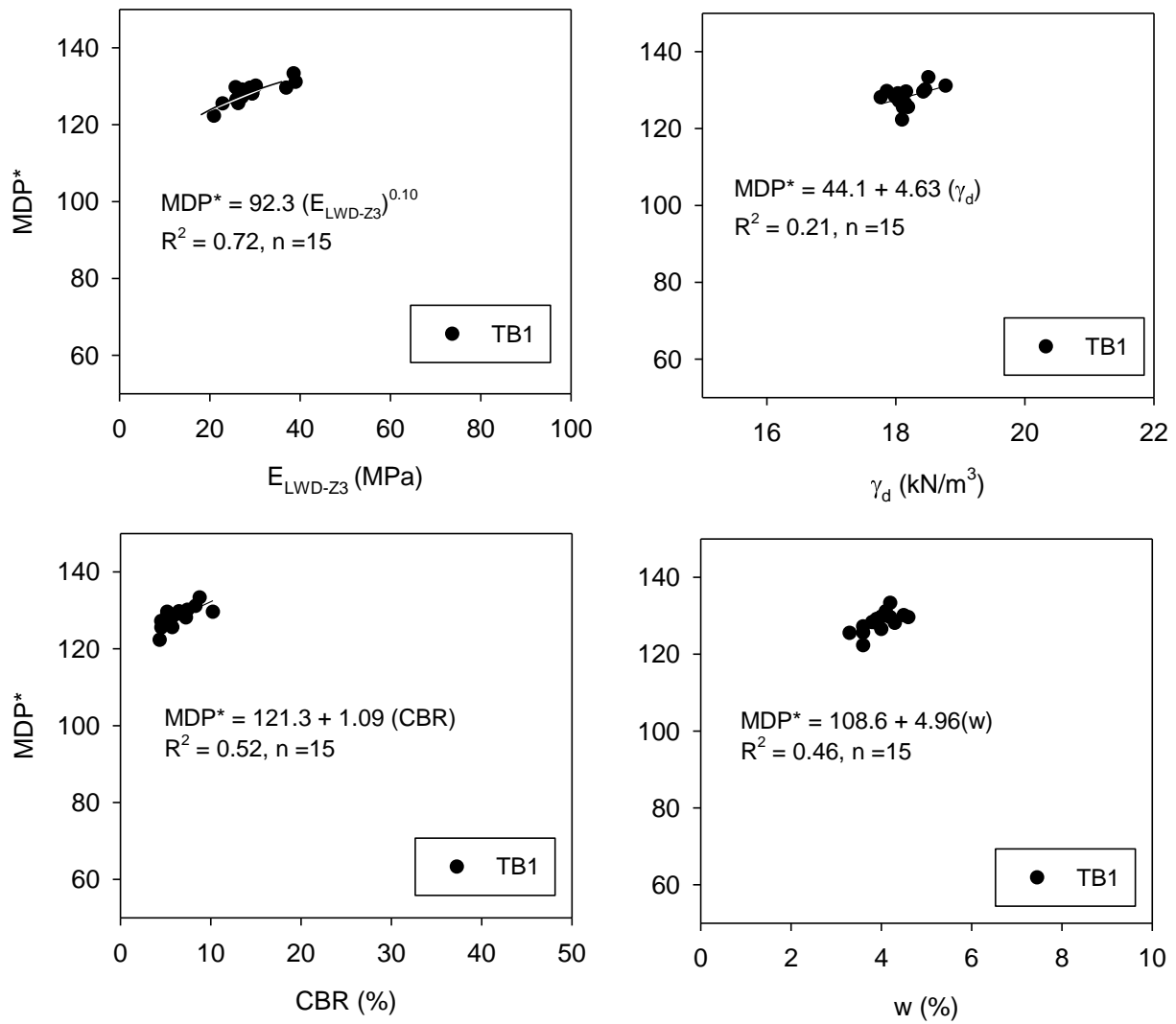
Figure 42. Correlations between MDP* and in-situ point-MVs – smooth drum roller with *a* = 1.80 mm setting (TB1 granular embankment fill)

41
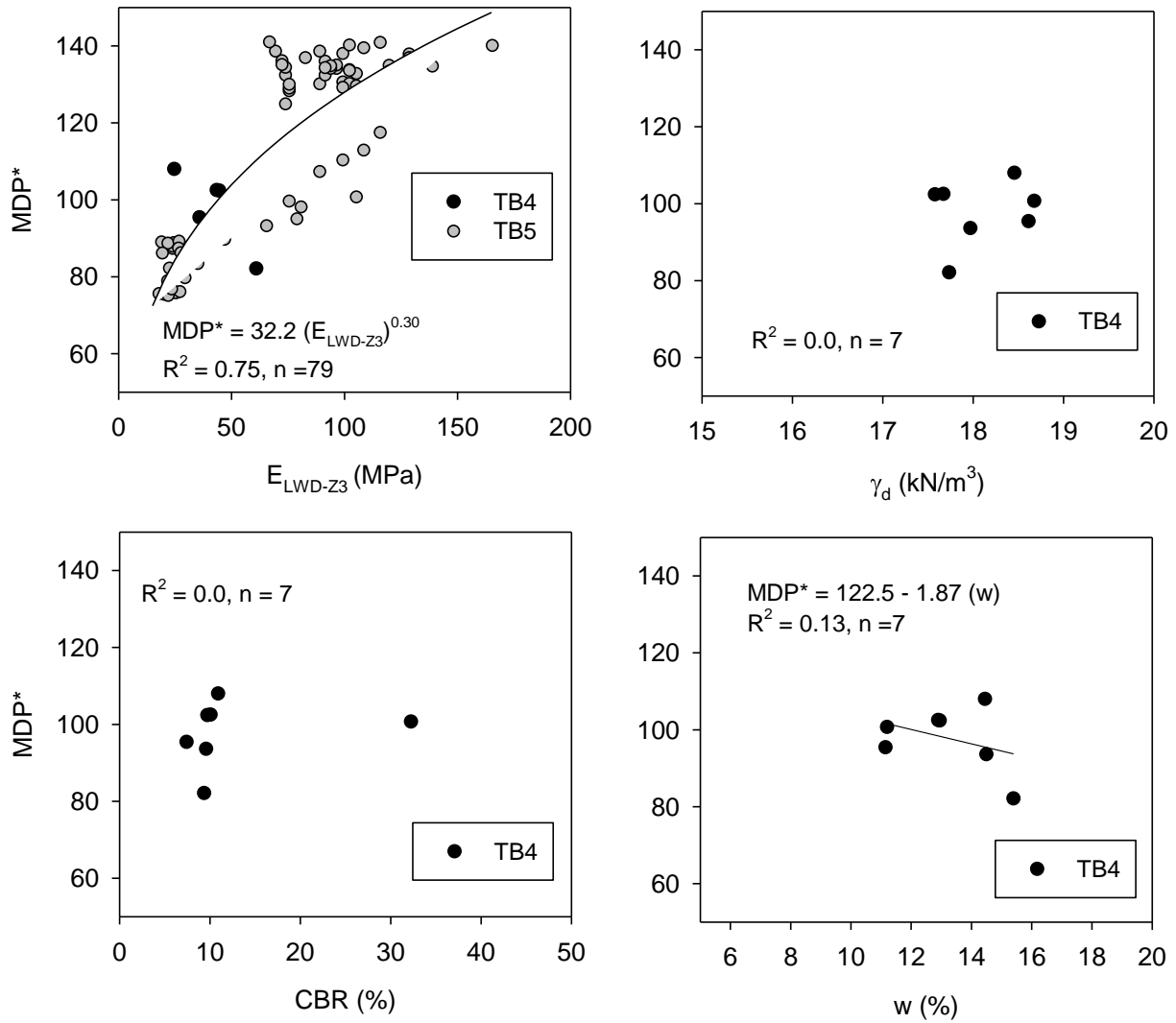
Figure 43. Correlations between MDP* and in-situ point-MVs – padfoot roller with static setting (TBs 4 and 5 cohesive embankment fill)
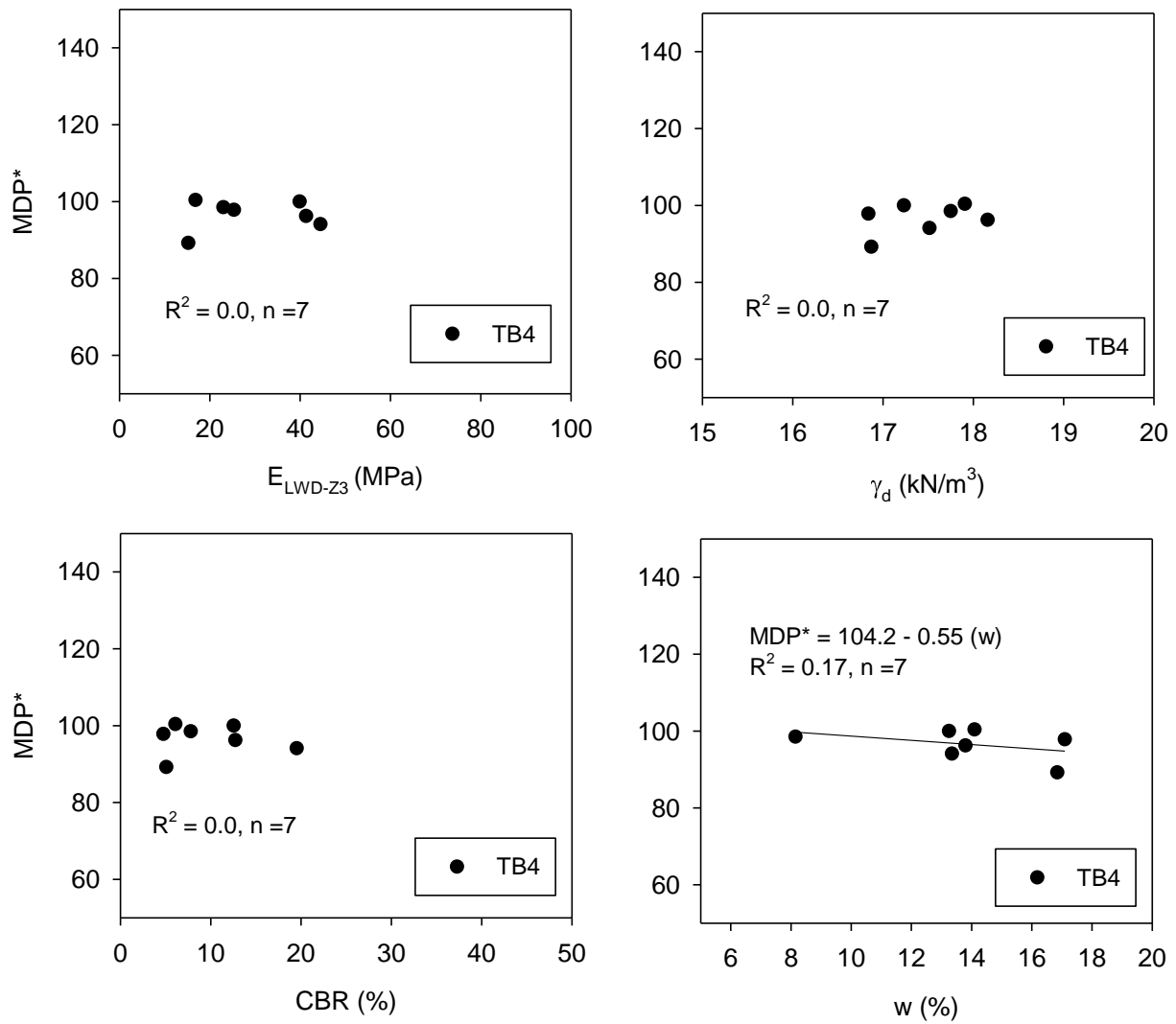
Figure 44. Correlations between MDP* and in-situ point-MVs – padfoot roller with *a* = 0.90 mm setting (TBs 4 and 5 cohesive embankment fill)

Field Demonstration – Open House

An open house was conducted on 08/19/2010 as part of this field investigation which included dissemination of results from previous IC field studies and results from the current field study as part of a presentation (Figure 45). A tour of the Iowa State University geotechnical mobile lab with several laboratory and in-situ testing methods followed the presentation. About 75 people attended the open house including Indiana DOT, contractor, and roller manufacturer personnel.

Figure 45. Photographs from open house on the project site

Contractor Interview

A contractor representative (Mr. Kevin Heini with Crider & Crider, Figure 46) was trained on site to make use of the on-board computer display during compaction operations on TB6 using CS563 smooth drum vibratory IC roller. After the roller operations, the research team interviewed him with the following questions and his responses are summarized as follows:

Figure 46. Contractor roller operator being interviewed after testing IC operations.

Question: "What to do you think about how the process worked and what information from the display was valuable and not valuable?"

> **Response:** *The on board display monitor was helpful to keep track of the number of roller passes. Also, by experience I know that there would be areas that are relatively soft than other areas just because there was no construction traffic on it."*

Question: "Does the IC values you see on the monitor confirm what you would expect from experience?"

> **Response:** *Yes. If you hit a thick lift spot, the IC values went down and if you hit a relatively thin lift spot, the IC values go up.*

Question: "What did you think about the display? Did you use the display much during compaction operations?"

> **Response:** *The display worked well. But when you do your first pass, it's all red, so cannot see the roller icon very well. It's a bit distracting as the screen moves when the station passes.*

Question: Would you give a thumbs up or a thumps down for the technology?

> **Response:** *I would give thumbs up and would be good for us to use it more.*

SUMMARY AND CONCLUSIONS

Results from a field study conducted on the SR25 near West Lafayette, Indiana, from August 16 to 18, 2010 are presented in this report. The project involved evaluating a Caterpillar CS-56 padfoot IC roller on cohesive embankment fill and a CS-563E smooth drum IC rollers on granular embankment fill materials. A total of six test beds involving calibration and production operations were constructed and tested as part of this study. MDP* IC-MVs were obtained from the test beds in conjunction with various in-situ point-MVs from nuclear gauge, LWD, and DCP test devices. IC-MVs maps on the on-board computer display unit were utilized in selecting field QA test locations to simulate a future specification option in some production areas. Some of the key findings and conclusions from this field study are provided below:

- Two IC rollers were used on this project: Caterpillar CS56 padfoot roller and a Caterpillar CS563E smooth drum vibratory roller. Both machine recorded machine drive power (MDP) and displayed the results on a computer screen in the roller cab. The MDP values obtained from the machine were scaled to range between 1 and 150. The reported MDP* value increases with increasing support capacity of the ground.

- Several in situ test methods were used to characterize compaction quality and for correlation analysis to the IC-MVs. Testing include the nuclear density gauge (NG) dry density and moisture content , dynamic cone penetrometer (DCP), and light weight deflectoemter (LWD).

- Several test strips were constructed with two different materials: A-7-6 (13) and A-3 materials. The padfoot roller was used to compact the cohesive material and the smooth drum to compact the sand material.

- Linear regression and geospatial analysis techniques were used to evaluate correlations between the IC-MVs and in situ point measurements. Results shows that the general trends were observed for most measurements, but that the E_{LWD} values were correlated best to the MDP values. Spatial analysis showed changes in semi-variance as a function of roller pass coverage and demonstrates an approach for characterizing spatial non-uniformity.

- According to the contractor operator, it would be good to use this technology more.

- It is recommended that additional pilot projects be established to further advance implementation of IC technology in Indiana and that additional work be focused on incorporating stiffness-based in situ measurements to supplement or replace nuclear density testing.

REFERENCES

ASTM D6951-03. (2003). "Standard test method for use of the dynamic cone penetrometer in shallow pavement application." American Standards for Testing Methods (ASTM), West Conshohocken, Pennsylvania.

ASTM D698-07e1. (2007). "Standard test method for laboratory compaction characteristics of soil using standard effort." American Standards for Testing Methods (ASTM), West Conshohocken, Pennsylvania.

ASTM D422-63. (2007). "Standard test method for particle-size analysis of soils." American Standards for Testing Methods (ASTM), West Conshohocken, Pennsylvania.

ASTM D4318-05 (2005). "Standard test methods for liquid limit, plastic limit, and plasticity index of soils." American Standards for Testing Methods (ASTM), West Conshohocken, Pennsylvania.

ASTM D3282-09. (2009). "Standard practice for classification of soils and soil-aggregate mixtures for high construction purposes." American Standards for Testing Methods (ASTM), West Conshohocken, Pennsylvania.

ASTM D2487-10. (2010). "Standard practice for classification of soils for engineering purposes (unified soil classification system)." American Standards for Testing Methods (ASTM), West Conshohocken, Pennsylvania.

Brandl, H., and Adam, D. (1997). "Sophisticated continuous compaction control of soils and granular materials." *Proc. 14th Intl. Conf. Soil Mech. and Found. Engrg.*, Hamburg, Germany, 1–6.

Chilès, J-P., and Delfiner, P. (1999). *Geostatistics – Modeling Spatial Uncertainty.* John Wiley & Sons, Inc., New York.

Clark, I., and Harper, W. (2002). *Practical geostatistics 2000.* 3rd reprint, Ecosse North America Llc, Columbus, Ohio.

Isaaks, E. H., and Srivastava, R. M. (1989). *An introduction to applied geostatistics.* Oxford University Press, New York.

Lambe, T. W., and Whitman, R. V. (1969). *Soil mechanics*, John Wiley & Sons, New York.

Mooney, M., Rinehart, R., White, D.J., Vennapusa, P., Facas, N., Musimbi, O. 2010. *Intelligent Soil Compaction Systems*, NCHRP 21-09 Final Report, National Cooperative Highway Research Program, Washington, D.C.

Samaras, A.A., Lamm, R., Treiterer, J. (1991). "Application of continuous dynamic compaction control for earthworks in railroad construction." *Transp. Res. Rec.,* 1309, Journal of the Transportation Research Board, Washington, D.C., 42–46.

Sandström, Å. (1994). *Numerical simulation of a vibratory roller on cohesionless soil,* Internal Report, Geodynamik, Stockholm, Sweden.

Sandström Å., and Pettersson, C. B., (2004). "Intelligent systems for QA/QC in soil compaction", *Proc. TRB 2004 Annual Meeting* (CD-ROM), Transportation Research Board, Washington, D. C.

Thompson, M., and White, D. (2008). "Estimating compaction of cohesive soils from machine drive power." *J. of Geotech. and Geoenv. Engrg.,* ASCE, 134(12), 1771-1777.

Vennapusa, P., White, D.J., and Gieselman, H. (2009). "Influence of support conditions on roller-integrated machine drive power measurements for granular base.", *Intl. Found. Cong. and Equip. Expo (IFCEE) 2009*, 15-19 March, Orlando, Florida.

Vennapusa, P., and White, D. J. (2009). "Comparison of light weight deflectometer measurements for pavement foundation materials." *Geotech.Test. J.*, ASTM, 32(3), 239-251.

Vennapusa, P., White, D.J., Morris, M. (2010). "Geostatistical analysis for spatially referenced roller-integrated compaction measurements, *J. of Geotech. and Geoenv. Engrg.,* ASCE, Vol. 136, No. 6, 813-822.

White, D. J., Jaselskis, E., Schaefer, V., Cackler, T. (2005). "Real-time compaction monitoring in cohesive soils from machine response." *Transp. Res. Rec., 1936*, Journal of the Transportation Research Board, Washington D.C., 173–180.

White, D.J., and Thompson, M. (2008). Relationships between in situ and roller-integrated compaction measurements for granular soils. *J. of Geotech. and Geoenv. Engrg.,* ASCE, 134(2), 1763-1770.

White, D., Thopmson, M., Vennapusa, P., and Siekmeier, J. (2008). "Implementing intelligent compaction specifications on Minnesota TH 64: Synopsis of measurement values, data management, and geostatistical analysis." *Transp. Res. Rec.,* 2045, Journal of the Transportation Research Board, Washington, D.C, 1-9.

White, D.J., Vennapusa, P., Zhang, J., Gieselman, H., Morris, M. (2009a). *Implementation of Intelligent Compaction Performance Based Specifications in Minnesota*, EERC PublicationER09-03, MN/RC 2009-14, Minnesota Department of Transportation, St. Paul, Minnesota, March.

White, D.J., Vennapusa, P., Gieselman, H., Johanson, L., Siekmeier, J. (2009b). "Alternatives to heavy test rolling for cohesive subgrade assessment," *Eighth Intl. Conf. on the Bearing Capacity of Roads, Railways, and Airfields (BCR2A'09)*, June 29 – July 2, Champaign, Illinois.

Zorn, G. (2003). *Operating manual: Light drop-weight tester ZFG2000*, Zorn Stendal, Germany.